THE MECHANISM OF PHASE TRANSFORMATIONS IN CRYSTALLINE SOLIDS

Proceedings of an International Symposium organized by the Institute of Metals and held in the University of Manchester from 3 to 5 July 1968

Monograph and Report Series
No. 33

1969
Published by
The Institute of Metals
17 Belgrave Square, London, S.W.1
for the Metals and Metallurgy Trust

First published 1969

Printed in Great Britain by BPC Letterpress Ltd., London, at Sidney Press, Bedford

CONTENTS

Session I: Spinodal Decomposition

Session II: Precipitation

Session III: Particle Coarsening

Session IV: Martensite

Session IV: Martensite, *continued*

Session V: Order–Disorder

Session VI: Interface-Controlled Transformations

Session VII: Theory of Transformations

PREFACE

In 1966 the Metallurgy Committee of the Institute of Metals initiated an international conference entitled "The Mechanisms of Phase Transformations in Crystalline Solids". The conference was held in the University of Manchester from 3 to 5 July 1968, with the following programme committee :

R. B. Nicholson (*Chairman*)	University of Manchester
J. W. Christian	University of Oxford
G. W. Greenwood	University of Sheffield
J. Nutting	University of Leeds
R. E. Smallman	University of Birmingham

The object of the conference was to discuss and correlate recent advances in the theory and experimental investigation of the mechanisms of phase transformations in crystalline solids.

This volume contains the introductory and contributed papers that were preprinted for the conference, research notes that were orally presented at the conference, and an edited version of the discussion that took place at the conference. The programme committee wishes to thank Dr. P. Wilkes and Dr. G. W. Lorimer of the University of Manchester for their considerable help in the recording and editing of the discussion.

Coherency Stress in Elastically Anisotropic Crystals and Its Effect on Diffusional Processes

John W. Cahn

Coherency strains from compositional inhomogeneities in elastically anisotropic cubic crystals are shown to have an anisotropic hydrostatic component. This affects the free energy and leads to a new term in the diffusion equation for coherent processes. The influence of this effect on nucleation, coarsening, homogenization, and spinodal decomposition is discussed.

Spinodal decomposition occurs by a spontaneous diffusion process. Diffusion in cubic crystals is usually isotropic, yet the spinodal reaction in such a crystal is not.[1] The anisotropy is the result of the introduction of elastic coherency terms that are not isotropic.

Coarsening of coherent precipitates is also a spontaneous diffusion process. It leads in cubic crystals to alignment of the remaining precipitates along certain crystallographic directions.[2,3] This is almost certainly the result of coupling anisotropic coherency strains to the diffusion process.

Symmetry rules for processes in crystals are quite basic and if we write

$$-J_i = \sum_{j=1}^{3} D_{ij} \frac{\partial c}{\partial x_j} \qquad (i = 1, 2, 3) \qquad \ldots (1)$$

for Fick's first diffusion equation, D_{ij} cannot be anything but isotropic[4] and equation (1) becomes

$$-\bar{J} = D\nabla c \qquad \ldots (2)$$

Equation (1) could be considered as the first term of an expansion for the flux $\bar{J}$ in terms of spatial derivatives of the composition c. In the spinodal theory we encounter an additional term

$$-J_i = \sum_{j=1}^{3} D^{(1)}_{ij} \frac{\partial c}{\partial x_j} + \sum_{j=1}^{3}\sum_{k=1}^{3}\sum_{l=1}^{3} D^{(2)}_{ijkl} \frac{\partial^3 c}{\partial x_j \partial x_k \partial x_l} \qquad (i = 1, 2, 3) \qquad \ldots (3)$$

Manuscript received 22 February 1968. Professor J. W. Cahn, Ph.D., is in the Department of Metallurgy and Materials Science, Massachusetts Institute of Technology, Cambridge, Mass., U.S.A.

$D^{(2)}$ is a tensor of rank four and could be anisotropic. Yet because it is the product of the diffusion and gradient energy coefficients, both second-rank tensors, it too is isotropic.[1,5,6] Thus equation (2) is not the correct form for introduring the elastic anisotropy. The present paper is a derivation of the appropriate diffusion equation that permits the introduction of elastic anisotropy.

Let us start with an expression for the free energy of a nonuniform, coherent system containing long-range composition fluctuations about an average composition c_0. This free energy is composed of three terms:[1,5]

(1) $F_{ch} = \int f'(c)\, dV$, the integral of the homogeneous free-energy density, $f'(c)$, which is the free energy that each element of volume of composition c would have if it were surrounded by homogeneous material of the same composition. The quantity $f'(c)$ is the free energy that we would measure in real, homogenized solid solutions by conventional means.

(2) F_G, the gradient energy, a first term in the expansion for additional energy that results from the effects of long-range composition gradients. A simple derivation of this term[6] compares the kinds of neighbours of an atom in a homogeneous material with those of an atom in a gradient but at a site of the same composition. For a general crystal system it must have the form

$$\sum_{i=1}^{3}\sum_{j=1}^{3} K_{ij} \frac{\partial c}{\partial x_i} \frac{\partial c}{\partial x_j} \qquad \ldots (4)$$

and K is a tensor of rank two. For cubic systems, K is isotropic[6] and the gradient energy reduces to $K(\nabla c)^2$.

(3) F_{el}, the elastic energy. If the lattice parameters are functions of composition, then a coherent inhomogeneous system will have additional elastic energy that may be calculated in a straightforward way from linear elasticity and, for isotropic elasticity, may be incorporated into the volume free energy.[7]

The model for calculating the elastic strain energy of a coherent system starts with a stress-free uniform crystal and assumes that we coherently produce a change in an element of volume at $\bar{\mathbf{r}}$ that would produce a strain $\varepsilon_{ij}(\bar{\mathbf{r}})$ if that element were kept stress-free. We also assume that the elastic constants are independent of this stress-free strain.

When the source of the stress-free strain is a composition change we may, for small composition excursions, define γ_{ij}, the strain produced by a unit composition change, and

$$\varepsilon_{ij}(\bar{\mathbf{r}}) = \gamma_{ij}\,[c(\bar{\mathbf{r}}) - c_0] \qquad \ldots (5)$$

For a cubic crystal $\gamma_{ij} = \gamma_i \delta_{ij}$ and

$$\gamma_i = \frac{\partial \ln a}{\partial c} \qquad \ldots (6)$$

where a is the lattice parameter. For such a case†

$$F_{el} = (2\pi)^3 \iiint [Y(\bar{\boldsymbol{\beta}})\, E(\bar{\boldsymbol{\beta}})\, E^*(\bar{\boldsymbol{\beta}})] d^3\bar{\boldsymbol{\beta}} \qquad \ldots (7)$$

$$= (2\pi)^3\, \gamma_i^2 \iiint [Y(\bar{\boldsymbol{\beta}})\, A(\bar{\boldsymbol{\beta}})\, A^*(\bar{\boldsymbol{\beta}})]\, d^3\bar{\boldsymbol{\beta}} \qquad \ldots (8)$$

where

$$Y(\bar{\boldsymbol{\beta}}) = \tfrac{1}{2}(C_{11} + 2C_{12}) \times \left[3 - \frac{C_{11} + 2C_{12}}{C_{11} + 2(2C_{44} - C_{11} + C_{12})(l^2m^2 + m^2n^2 + n^2l^2)}\right] \qquad \ldots (9)$$

is an orientation-dependent elastic modulus where l, m, and n are the directional cosines that $\bar{\boldsymbol{\beta}}$ makes with the cube axes. E (and E^*) and A (and A^*) are respectively the complex Fourier transforms (and their complex conjugates) of ε and c.

$$E(\bar{\boldsymbol{\beta}}) = \left(\frac{1}{2\pi}\right)^3 \iiint \varepsilon(\bar{\mathbf{r}}) \exp(i\bar{\boldsymbol{\beta}} \cdot \bar{\mathbf{r}})\, d^3\bar{\boldsymbol{\beta}} \qquad \ldots (10)$$

$$A(\bar{\boldsymbol{\beta}}) = \left(\frac{1}{2\pi}\right)^3 \iiint (c(\bar{\mathbf{r}}) - c_0) \exp(i\bar{\boldsymbol{\beta}} \cdot \bar{\mathbf{r}})\, d^3\bar{\mathbf{r}} \qquad \ldots (11)$$

where $\bar{\boldsymbol{\beta}}$ is a wave vector and $\bar{\mathbf{r}}$ the position vector in the specimen. The quantity $A(\bar{\boldsymbol{\beta}})$ is independent of how fine a scale we choose for smoothing, provided that the reciprocal of this scale length is larger than $\bar{\boldsymbol{\beta}}$. We conveniently do this by putting an upper limit to $\bar{\boldsymbol{\beta}}$ in the integral.

F_{el} differs from the atomic-misfit energy that occurs in solid-solution theory and originates from fitting together atoms of different sizes.[8,9] This atomic-misfit energy is implicitly included in f' as measured; it is the difference between f' of a real, homogeneous solution and a free energy of a hypothetical solution of the same system in which all the atoms have the same size (Fig. 1). Although this hypothetical solution may have a certain theoretical fascination, it cannot be made in the laboratory or measured and is of no use as a starting point for a phenomenological theory. F_{el} on the other hand is the difference between two real free energies, that of a coherent system and a system with the same phases or compositions separated into stress-free portions. As shown in Fig. 2, these two elastic energies have apparently opposite effects[9] in promoting precipitation but since curve c is an unrealizable state, it is immaterial whether or not such a hypothetical solution would have a miscibility gap. In Figs. 1 and 2, curves b and c have a tendency to be parallel. This is especially true if we use atomic-misfit theories[8] in which each atom of a solid solution is assumed to be a region of composition 0 or 1 coherently joined to every other atom.

The sum of the three terms, F_{ch}, F_G, and F_{el}, is the free energy of a non-uniform system and by differentiating this sum we obtain an expression for the free-energy change resulting from an arbitrary infinitesimal change in the composition anywhere, $\delta c(\bar{\mathbf{r}})$,

$$\delta F = \iiint \left[\frac{\partial f'}{\partial c} - 2K\nabla^2 c - \frac{\partial K}{\partial c}(\nabla c)^2 + 2\gamma_i^2 \iiint A\, Y \exp(-i\bar{\boldsymbol{\beta}} \cdot \bar{\mathbf{r}})\, d^3\bar{\boldsymbol{\beta}}\right] \delta c(\bar{\mathbf{r}})\, d^3\bar{\mathbf{r}} \qquad \ldots (12)$$

†The derivation in Ref. (1) considers a single sine wave. The factor $(2\pi)^3$ instead of V originates in the passage to a continuous distribution of wavelengths in an infinite system.

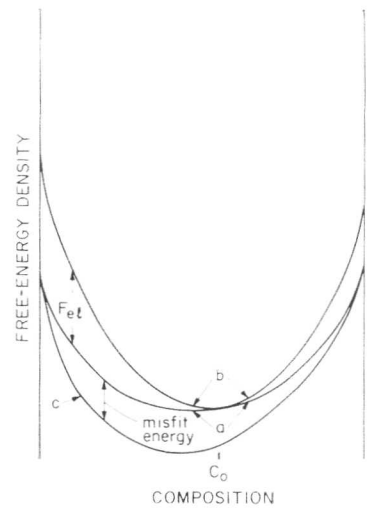

Fig. 1 Schematic free energy vs. composition curves illustrating the distinction between the effects of coherency strains and atomic misfit energy. Curve (a) *is the actual free energy of a mole of homogeneous solution as a function of composition. Curve* (b) *is the actual free energy per mole of a small amount of homogeneous solution of composition* c *coherently enclosed in a matrix of average composition* c_0. *The difference between these curves is the elastic energy due to coherency. Curve* (c) *is a hypothetical solution of the atoms identical to the actual solution except that the atoms are all assumed to have the same size. The difference between curves* (a) *and* (c) *is the atomic misfit energy.*

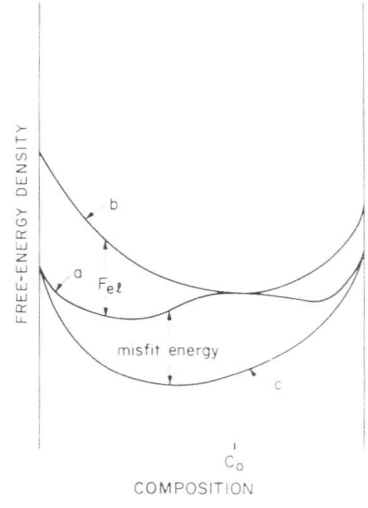

Fig. 2 Schematic free-energy curves to illustrate that while the atomic-misfit energy is a factor that reduces solubility, the coherency strain is a factor reducing the tendency for a supersaturated solution to precipitate coherently. Curves (a), (b), *and* (c) *have the same meanings as in Fig. 1.*

The variational derivative of F, the derivative of free energy with respect to a change in c at $\bar{\mathbf{r}}$, is

$$\frac{\delta F}{\delta c} = \frac{\partial f'}{\partial c} - 2K\nabla^2 c - \frac{\partial K}{\partial c}(\nabla c)^2 + 2\eta^2 \iiint A\, Y \exp(-i\bar{\boldsymbol{\beta}}.\bar{\mathbf{r}}) d^3\bar{\boldsymbol{\beta}} \quad \ldots (13)$$

The hydrostatic portion of the stress field $p(\bar{\mathbf{r}})$ can similarly be expressed as a variational derivative of F_{el} with respect to $\varepsilon(\bar{\mathbf{r}})$

$$p(\bar{\mathbf{r}}) = \frac{\delta F_{el}}{\delta \varepsilon} = 2 \iiint E(\bar{\boldsymbol{\beta}})\, Y(\bar{\boldsymbol{\beta}}) \exp(-i\bar{\boldsymbol{\beta}}.\bar{\mathbf{r}})\, d^3\bar{\boldsymbol{\beta}} \quad \ldots (14)$$

The interdiffusional flux may be written

$$-\bar{J} = M\nabla \frac{\delta F}{\delta c} \quad \ldots (15)$$

where M is a tensor of rank two defined phenomenologically by this equation. By taking the divergence

$$-\nabla.\bar{J} = \frac{\partial c}{\partial t} = \nabla.M\nabla \frac{\delta F}{\delta c} \quad \ldots (16)$$

Introducing the variational derivative, performing the indicated differentiation and ignoring non-linear terms, we obtain

$$-\bar{J} = M\frac{\partial^2 f'}{\partial c^2}\nabla c - 2MK\nabla^3 c + 2\eta^2 \iiint (-i\bar{\boldsymbol{\beta}}) A\, Y \exp(-i\bar{\boldsymbol{\beta}}.\bar{\mathbf{r}})\, d^3\bar{\boldsymbol{\beta}} \quad \ldots (17)$$

and

$$\frac{\partial c}{\partial t} = M\frac{\partial^2 f'}{\partial c^2}\nabla^2 c - 2MK\nabla^4 c + 2\eta^2 \iiint (-i\bar{\boldsymbol{\beta}})^2 A\, Y \exp(-i\bar{\boldsymbol{\beta}}.\bar{\mathbf{r}})\, d^3\bar{\boldsymbol{\beta}} \quad \ldots (18)$$

Several interesting effects result from the discarded non-linear terms. Of these, the effects of composition or strain on the diffusion coefficient[10] and elastic coefficients[3] have been discussed elsewhere.

These equations can be solved readily by a Fourier transform of the compositional terms. Inserting equation (11) into (18) we obtain

$$\frac{\partial A}{\partial t} = -\beta^2 M\left[\frac{\partial^2 f'}{\partial c^2} + 2\eta^2 Y(\bar{\boldsymbol{\beta}}) + 2K\beta^2\right] A \quad \ldots (19)$$

and upon integration

$$A(\bar{\boldsymbol{\beta}},t) = A(\bar{\boldsymbol{\beta}},0)\exp\left(-\beta^2 M\left[\frac{\partial^2 f'}{\partial c^2} + 2\eta^2 Y(\bar{\boldsymbol{\beta}}) + 2K\beta^2\right] t\right) \quad \ldots (20)$$

where $A(\bar{\boldsymbol{\beta}},t)$ and $A(\bar{\boldsymbol{\beta}},0)$ are, respectively, the Fourier transform of the composition at time t and at time 0. Equation (20) is the solution to the diffusion equation (18) as it appears in the theory of spinodal decomposition. The quantity in the brackets in the exponent is an orientation-dependent diffusional amplification factor. The anisotropic term depends on the square of the wave number, just as if it originated in $D^{(1)}$ of equation (3). $D^{(1)}$ is, however, isotropic and in equations (17) and (18) the anisotropic term appears as a Fourier transform. Let us now perform the indicated transformation of the anisotropic elastic term in equations (13), (14), (17), and (18) and express these equations entirely in c (or ε) and its derivatives. The method of performing this transformation is shown in the Appendix. The results are

$$\frac{\delta F}{\delta c} = \frac{\partial f'}{\partial c} - 2K\nabla^2 c - \frac{\partial K}{\partial c}(\nabla c)^2 + 2\bar{Y}\eta^2(c(\bar{\mathbf{r}}) - c_0) - \frac{\eta^2}{2\pi}\sum_{l=1}^{\infty}\sum_{m=-l}^{l}(-i)^l C_l\, y_{lm} \iiint \frac{\nabla^2 c(\bar{\mathbf{r}} - \bar{\mathbf{r}}')\; Y_{lm}(\theta',\varphi')\, d^3\bar{\mathbf{r}}'}{\bar{\mathbf{r}}'} \quad \ldots (21)$$

$$-\bar{J} = M\left[\left(\frac{\partial^2 f'}{\partial c^2} + 2\eta^2\bar{Y}\right)\nabla c - 2K\nabla^3 c - \frac{\eta^2}{2\pi}\sum_{l=1}^{\infty}\sum_{m=-1}^{l}(-i)^l C_l y_{lm} \iiint \frac{\nabla^3 c(\bar{\mathbf{r}} - \bar{\mathbf{r}}')\; Y_{lm}(\theta',\varphi') d^3\bar{\mathbf{r}}'}{\bar{\mathbf{r}}'}\right] \quad \ldots (22)$$

$$\frac{\partial c}{\partial t} = M\left[\left(\frac{\partial^2 f'}{\partial c^2} + 2\eta^2\bar{Y}\right)\nabla^2 c - 2K\nabla^4 c - \frac{\eta^2}{2\pi}\sum_{l=1}^{\infty}\sum_{m=-1}^{l}(-i)^l C_l y_{lm} \iiint \frac{\nabla^4 c(\bar{\mathbf{r}} - \bar{\mathbf{r}}')\, Y_{lm}(\theta',\varphi') d^3\bar{\mathbf{r}}'}{\bar{\mathbf{r}}'}\right] \quad \ldots (23)$$

$$p(\bar{\mathbf{r}}) = 2\bar{Y}\varepsilon(\bar{\mathbf{r}}) - \frac{1}{2\pi}\sum_{l=1}^{\infty}\sum_{m=-l}^{l}(-i)^l C_l\, y_{lm} \times \iiint \frac{\nabla^2\varepsilon(\bar{\mathbf{r}} - \bar{\mathbf{r}}')\; Y_{lm}(\theta',\varphi') d^3\bar{\mathbf{r}}'}{\bar{\mathbf{r}}'} \quad \ldots (24)$$

In each of these equations there appears a term describing an effect at point $\bar{\mathbf{r}}$ resulting from strains everywhere else in the system. These effects are described in terms of a convolution integral, an integral over all elements of volume a distance $\bar{\mathbf{r}}'$ away from the point $\bar{\mathbf{r}}$. In this form the anisotropy enters in a manner that clearly does not violate crystal symmetry.

Discussion

The hydrostatic component of the coherency stress at $\bar{\mathbf{r}}$ (equation (24)) arises from both the value of the stress-free strain ε at $\bar{\mathbf{r}}$, and a long-range anisotropic term that depends on the Laplacian of ε at a vector distance $\bar{\mathbf{r}}'$ from $\bar{\mathbf{r}}$ multiplied by an elastic influence factor (Fig. 3) that is a function of the orientation of $\bar{\mathbf{r}}'$ and inversely proportional to its magnitude equation (24)). As shown in equation (A8), this orientation-dependent term approximately parallels the orientation-dependence of $Y(\bar{\boldsymbol{\beta}})$ except that the former oscillates about zero. It is zero for an elastically isotropic crystal; otherwise it is positive or negative for orientations where $Y(\bar{\boldsymbol{\beta}})$ is respectively greater or less than its average value $\bar{Y}$. Like $Y(\bar{\boldsymbol{\beta}})$, it has minima or maxima for elastically soft or hard directions: at (111) and (100), respectively, if $C_{44} < (C_{11} - C_{12})/2$, and at (100) and (111), respectively, if $C_{44} > (C_{11} - C_{12})/2$.

For an elastically isotropic system with constant elastic coefficients only the first term survives. This leads to the absence of elastic interaction between centres of dilatational strain, a result that was first derived by Crum.[8,11] However, elastic coefficients that are functions of $\varepsilon(\bar{\mathbf{r}})$ (through the composition by equation (5)) lead to an interaction between centres of strain. In the diffusion equation these survive only as non-linear terms.

As a result of the hydrostatic component, coherency strains in cubic crystals have both a local and a long-range influence on diffusion (equations (22) and (23)). In an elastically isotropic crystal there is no long-range component and the diffusional flux at $\bar{\mathbf{r}}$ depends only on $\varepsilon(\bar{\mathbf{r}})$ or $[c(\bar{\mathbf{r}}) - c_0]$.

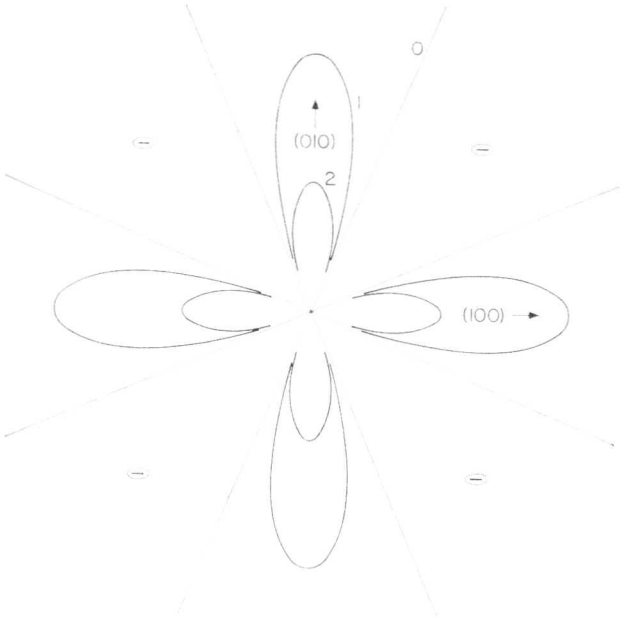

Fig. 3 A plot of the (001) *plane showing contours of equal positive values of* $(Y_{44} + Y_{4\bar{1}})/r'$ *to illustrate the spatial dependence of the anisotropic elastic interaction.*

The main effect of elastic anisotropy is in the convolution integrals. The diffusional flux at $\bar{\mathbf{r}}$ now depends not only on the presence of nearby causes of strain but on their orientation and distance relative to $\bar{\mathbf{r}}$. This anisotropic effect gives rise to the directionality in spinodal decomposition.[1] It is also the effect that gives rise to directionality in precipitation and ripening.[2,3] To see this most clearly, consider that the free energy of a particle at $\bar{\mathbf{r}}$ contains an elastic term that depends on a product of $\varepsilon(\bar{\mathbf{r}})$ and $p(\bar{\mathbf{r}})$. The isotropic portion of the latter is independent of the presence of other particles and is the same for all particles, but the anisotropic portion shows that a particle has preference for other particles (with similar strain) that are nearby and in soft directions. This anisotropic portion will lead to differences in " volume free energy " among particles

$$\Delta F_V = \Delta f' + \bar{Y}\,\varepsilon^2(\bar{\mathbf{r}}) - \frac{3}{32\pi}\,\varepsilon(\bar{\mathbf{r}}) \times \iiint_{\bar{\mathbf{r}}'} \frac{\nabla^2\varepsilon(\bar{\mathbf{r}} - \bar{\mathbf{r}}')\,(Y(\bar{\mathbf{r}}') - \bar{Y})\,d^3\bar{\mathbf{r}}'}{\bar{\mathbf{r}}'} \quad \ldots (25)$$

The last term in equation (25) covers all space and includes interactions among different parts of the same particle. By equation (25) the lowest " volume free energy " is a plate-like particle lying in a soft plane. A raft of separated particles on the same plane would have a similar low elastic energy.

If we now consider also the specific free energy σ of coherent interfaces, we should find that equilibrium particles are not spherical and that their equilibrium is affected by neighbouring particles. The quantity σ has no contribution from the coherency strains which behave as a " volume free energy ". Only small particles can be fully coherent, unless these strains are zero, and σ must be determined from measurements on small particles.

An approximate estimate of the effect of neighbouring particles on the nucleation rate and solubility of small particles can be made by assuming that the nucleating particles are spherical and small compared to their neighbours. Then the main contribution to the last term of equation (25) comes from the neighbouring particles. The " volume free energy " $(-\Delta F_V)$ is large for a particle nucleating nearby and in a soft direction to a similar particle. Consider such a small β particle in an α matrix with radius R at $\bar{\mathbf{r}}$. Setting $\Delta F_V = -2\sigma/R$

$$\Delta f' = \left(c_\beta^c - c_\alpha^c\right) N_V k T \ln\left[c_\alpha(\bar{\mathbf{r}})/c_\alpha^c\right]$$

where c_β^c and c_α^c are mole fractions of α and β in stress-free equilibrium and $c_\alpha(\bar{\mathbf{r}})$ is the concentration in α at equilibrium with the coherent β particle at $\bar{\mathbf{r}}$, we obtain approximately

$$\ln\left[c_\alpha(\bar{\mathbf{r}})/c_\alpha^c\right] = \frac{1}{N_V k T (c_\alpha^c - c_\beta^c)}\left\{\frac{2\sigma}{R} + \bar{Y}\varepsilon_\beta^2 - \frac{3}{32\pi}\iiint_{\bar{\mathbf{r}}'} \frac{\nabla^2\varepsilon(\bar{\mathbf{r}} - \bar{\mathbf{r}}')\,(Y(\bar{\mathbf{r}}') - \bar{Y})d^3\bar{\mathbf{r}}'}{\bar{\mathbf{r}}'}\right\} \quad \ldots (26)$$

where ε_β is the stress-free strain of forming a β particle. The first term is the usual Gibbs–Thomson effect. The remaining two are modifications required by the elastic energy; they lead to lower solubilities (and hence increased stability) for small particles in the elastically favoured positions.

Since, at large distances, the number of particles in a range dr varies as r^2, the convergence of the convolution integral depends on a random angular distribution of $\varepsilon(\bar{\mathbf{r}})$ or $[c(\bar{\mathbf{r}}) - c_0]$ at large distances. In coherent precipitation, this is automatically satisfied if we start with a large homogeneous crystal.

Obtaining the solution of the diffusion equation presents no great difficulty in spinodal decomposition. A Fourier transform of equation (23) leads directly to equation (19). For many purposes this equation is the useful solution. X-ray diffraction experiments lead directly to the Fourier transform of the composition and permit a direct verification of equation (19).[12] Several approximate methods exist to perform the inverse transformation of equation (20) and obtain the composition as a function of time. In spinodal decomposition the simplest is to assume that by selective amplification the fastest-growing Fourier components dominate. The resulting prediction is a structure composed of a sum of only a few Fourier components.[1,13] The typical tweed structure of (100) waves (or (111) waves, depending on elastic anisotropy alone) is the predicted result in anisotropic cubic crystals unless $\gamma_i = 0$.

The role of elastic anisotropy on coarsening kinetics has been qualitatively outlined through their influence on both critical radii and diffusion. Whether a simple modification of the existing theories of coarsening can incorporate these effects, or whether a Fourier method is required,[10] remains to be seen.

Acknowledgements

The author has benefited throughout this study from stimulating discussions with Kenneth C. Russell and Keith H. Johnson, and is especially grateful to the latter for valuable advice about the methods used in the Appendix. He also wishes to thank the National Science Foundation for a grant under which the work was performed.

Appendix

A transformation of a product of two terms is the convolution of the transforms of the individual factors. The transform of Y/β^2 is readily evaluated, while the transform of Y itself presented some difficulty except for the isotropic case where Y is a constant. Because of this, the factors in equations (13), (17), and (18) should be regrouped as follows:

$$\iiint \left[(-i\,\bar{\beta})^{2+n} A(\bar{\beta})\right] [Y/\beta^2] \exp(-i\,\bar{\beta}.\bar{r})\, d^3\beta = \left(\frac{1}{2\pi}\right)^3 \nabla^{2+n} c(\bar{r})^* \; \mathcal{F}^{-1}(Y/\beta^2) \qquad \ldots (A1)$$

To evaluate this transform, we expand $\exp(i\,\bar{\beta}.\bar{r})$ and $Y(\beta)$ in terms of normalized spherical harmonics Y_{lm} and a spherical Bessel function j_l. Let the spherical coordinates of $\bar{\beta}$ and $\bar{r}$ be $(\beta, \theta'', \varphi'')$ and (r, θ, φ). Then[14]

$$\exp(-i\,\bar{\beta}.\bar{r}) = 4\pi \sum_{l=0}^{\infty} \sum_{m=-l}^{l} (-i)^l j_l(\beta r)\, Y_{lm}^*(\theta'', \varphi'')\, Y_{lm}(\theta, \varphi) \qquad \ldots (A2)$$

$$Y(\bar{\beta}) = \sum_{l'=0}^{\infty} \sum_{m'=-l'}^{l'} y_{l'm'}\, Y_{l'm'}(\theta'', \varphi'') \qquad \ldots (A3)$$

where

$$y_{l'm'} = \int_0^{2\pi} \int_0^{\pi} Y(\bar{\beta})\, Y_{l'm'}^*(\theta'', \varphi'') \sin\theta''\, d\theta''\, d\varphi'' \ldots (A4)$$

The integrals of the Bessel function are

$$\int_0^{\infty} j_0(\beta r)\, d\beta = \pi/2r$$

and for l even

$$\int_0^{\infty} j_l(\beta r)\, d\beta = \frac{l-1}{l} \int_0^{\infty} j_{l-2}(\beta r)\, d\beta = \pi C_l/2r \qquad \ldots (A5)$$

where

$$C_l = \frac{1 \cdot 3 \cdot 5 \ldots (l-1)}{2 \cdot 4 \cdot 6 \ldots l}$$

Making use of the orthogonality relations among the Y_{lm} we obtain

$$\mathcal{F}^{-1}(Y/\beta^2) = \iiint (Y/\beta^2) \exp(-i\,\bar{\beta}.\bar{r})\, d^3\bar{\beta} = 2\pi^2/r \left[\bar{Y} + \sum_{l=1}^{\infty} \sum_{m=-l}^{l} (-i)^l C_l\, y_{lm}\, Y_{lm}\right]$$

where $\qquad \ldots (A6)$

$$\bar{Y} = \frac{1}{4\pi} \int_0^{2\pi} \int_0^{\pi} Y(\bar{\beta}) \sin\theta''\, d\theta''\, d\varphi'' \qquad \ldots (A7)$$

is the spherical average value of $Y(\bar{\beta})$. When this is substituted into equation (A1) the first term in the expansion is readily integrated by means of Green's Theorem to give

$$\iiint (-i\,\bar{\beta})^n A Y \exp(-i\bar{\beta}.\bar{r})\, d^3\bar{\beta} = \bar{Y} \nabla^n c(\bar{r}) - \frac{1}{4\pi} \sum_{l=1}^{\infty} \sum_{m=-l}^{l} (-i)^l C_l\, y_{lm} \iiint \frac{\nabla^{2+n} c(\bar{r} - \bar{r}')\, Y_{lm}(\theta', \varphi')\, d^3\bar{r}'}{\bar{r}'} \qquad \ldots (A8)$$

For the isotropic case, Y is a constant $\bar{Y}$ and only this first term survives. In this situation, Y could have been taken out of the integral in equation (A1) giving the same first term directly. Equation (A8) can be combined with (16), (17), and (18) to give equations (21), (22), and (23). Using equation (A6) the hydrostatic component of the stress given by equation (14) can be found and is given by equation (24). Because of cubic symmetry the only non-zero y_{lm} in these equations are (0,0), (4,0), (4,4), (6,0), (6,4), (8,0), &c. An alternate expansion in terms of Kubic harmonics[15] composed only of combinations of the allowed y_{lm} would lead to the same result.

An approximate evaluation of equation (A8) can be made by recognizing that the essential features of the anisotropy of $Y(\beta)$, the maxima and minima at (100) and (111), are described by the "$l = 4$" harmonics. Assuming that we have only the "$l = 0$" and "$l = 4$" terms, we may combine equations (A3) and (A8) to obtain approximately

$$\iiint (-i\,\bar{\beta})^n A Y \exp(-i\,\bar{\beta}.\bar{r})\, d^3\bar{\beta} = Y \nabla^n c(\bar{r}) - \frac{3}{32\pi} \iiint \frac{(Y(\bar{r}') - \bar{Y}) \nabla^{2+n} c(\bar{r} - \bar{r}')\, d^3\bar{r}'}{\bar{r}'} \qquad \ldots (A9)$$

and the anisotropy in equations (A8) and (21)–(24) parallels that of the deviation of Y from it spherical average $\bar{Y}$.

References

1. J. W. Cahn, *Acta Met.*, 1962, **10,** 179.
2. V. A. Phillips, *ibid.*, 1966, **14,** 1533.
3. A. J. Ardell, R. B. Nicholson, and J. D. Eshelby, *ibid.*, p. 1295.
4. J. F. Nye, "Physical Properties of Crystals", p. 20. **1957:** Oxford (Clarendon Press).
5. J. W. Cahn, *Acta Met.*, 1961, **9,** 795.
6. J. W. Cahn and J. E. Hilliard, *J. Chem. Physics*, 1958, **28,** 258.
7. J. W. Cahn, *Acta Met.*, 1962, **10,** 907; 1966, **14,** 83.
8. J. W. Christian, "The Theory of Transformations in Metals and Alloys", p. 188. **1965:** Oxford (Pergamon Press).
9. A. G. Khachaturyan, *Soviet Physics—Crystallography*, 1965, **10,** 248.
10. J. W. Cahn, *Acta Met.*, 1966, **14,** 1685.
11. F. R. N. Nabarro, *Proc. Roy. Soc.*, 1940, [A,] **175,** 519.
12. K. B. Rundman and J. E. Hilliard, *Acta Met.*, 1967, **15,** 1025.
13. J. W. Cahn, *J. Chem. Physics*, 1965, **42,** 93.
14. G. Goertzel and N. Tralli, "Some Mathematical Methods of Physics", p. 160. **1960:** New York and London (McGraw-Hill).
15. A. A. Maradudin, E. W. Montroll, and G. H. Weis, "Solid State Physics", Suppl. 3, (edited by F. Seitz and D. Turnbull) p. 97. **1963:** New York (Academic Press).

Spinodal Decomposition: Observations in the Isotropic, Non-Crystalline Na_2O–SiO_2 System

M. Tomozawa, H. Herman, and R. K. MacCrone

The unmixing or phase separation in the unstable range of various Na_2O SiO_2 glass systems has been investigated using small-angle X-ray scattering. By following the time development of the Fourier amplitudes of the composition fluctuations as unmixing occurs, phase separation by the spinodal mode has been identified. The behaviour of specimens with significant phase separation is in agreement with theory. At the initial stage of unmixing, quantitative agreement with certain aspects of the theory is obtained, but the inherent experimental difficulties preclude detailed correlation at this time. The diffusion coefficient obtained from the X-ray observation of the phase separation indicates that anion motion is the rate-controlling process during decomposition.

A gap in miscibility can occur in certain glass systems. When the initially homogeneous glass solution is cooled from the single-phase region to within the gap, unmixing is favoured, and two vitreous, conjugate phases can form. The new vitreous-product phases are of course metastable, but they persist by reason of the difficulty in achieving devitrification.

A supersaturated glass will phase separate ideally in one of three distinct ways:

(1) Devitrification (nucleation and development of a crystallized phase).

(2) Nucleation and growth of a second glass phase.

(3) Spinodal decomposition.

Devitrification will be excluded from consideration in this study; indeed, it is rather difficult to crystallize glass by simple heat-treatment. Thus we wish to distinguish between a process of nucleation and growth, and spinodal decomposition.

With regard to spinodal decomposition, it has been common in the past to employ the prediction of spatial connectivity between the two conjugate-product phases as evidence for the operation of this mode.[1] But connectivity of precipitates can also occur when only nucleation and growth is operating: connectivity develops from simple topological considerations whenever the volume fractions of the two phases are comparable. The assertion of spinodal decomposition based solely on this observation should therefore be treated with caution. In addition, in crystalline systems there is normally a dependence of specific volume on concentration. As phase separation by a spinodal mode proceeds, strain energy will contribute to the total free energy and this will introduce crystallographic directionality, resulting in the modulated structure so characteristic of this process. However, this morphology again cannot be unequivocally attributed to spinodal decomposition, since an interaction elastic-strain energy, associated with particles formed due to nucleation and growth, can also lead to a periodic array.[2] The question of strain energy does not arise in glass and need not be considered here.

Thus in this work we examine the kinetics of phase decomposition, and not the resulting morphology. We have studied the kinetics by examining the development of small-angle X-ray spectra during the early stage of decomposition. It will be shown that this change in X-ray spectra is intimately related to the development of compositional fluctuations in the specimen.

In Cahn's[3] formulation for a two-component fluid system, the concentration (atomic fraction), c, of solute at a position vector, $\mathbf{r}$, is written as a function of time as a Fourier integral:

$$c(\mathbf{r}, t) - c_0 = (1/2\pi)^3 \int_{\beta} A(\boldsymbol{\beta}, t) \exp [i\boldsymbol{\beta}.\mathbf{r}] d\boldsymbol{\beta} \quad \ldots (1)$$

where c_0 is the average composition, and $\boldsymbol{\beta}$ is the wave number, a vector in reciprocal space ($|\boldsymbol{\beta}| = 2\pi/\lambda$). $A(\boldsymbol{\beta}, t)$ is the Fourier amplitude of the expansion of the varying concentration, formally given by:

$$A(\boldsymbol{\beta}, t) = \int_{v} [c(\mathbf{r}, t) - c_0] \exp [-i\boldsymbol{\beta}.\mathbf{r}] \, d\mathbf{r} \quad \ldots (2)$$

where the integral is over the volume of the specimen. In this theoretical development, only those Fourier amplitudes (which describe the composition inhomogeneities of the specimen) within a range of wavelengths increase in magnitude with time during decomposition by a spinodal mode; outside this range, the amplitudes of the other Fourier components decay. The wavelength of the Fourier component that grows at the maximum rate is determined by various parameters of the system, and it is this spacing that, ideally, will ultimately predominate and that will characterize the decomposition morphology of the system.

Manuscript received 27 February 1968. M. Tomozawa, B.S., and H. Herman, B.S., M.S., Ph.D., are in the Laboratory for Research on the Structure of Matter, School of Metallurgy and Materials Science, University of Pennsylvania, Philadelphia, U.S.A., where the work was carried out. R. K. MacCrone, M.Sc., D.Phil., is now in the Division of Materials Engineering, Rensselaer Polytechnic Institute, Troy, New York.

Cahn has shown that a particular Fourier amplitude undergoes a development with time given by

$$A(\beta, t) = A(\beta, 0) \exp [R(\beta)\, t] \qquad \ldots (3)$$

where $R(\beta) = -D\beta^2 - 2M\varkappa\beta^4/N_v$ $\ldots (4)$

where D is the interdiffusion coefficient when no strains are present and M the mobility given by

$$M = N_v D (\partial^2 F/\partial c^2)^{-1} \qquad \ldots (5)$$

where N_v is the atomic density, and F is the Helmholtz free energy. The second derivative of F with respect to composition represents the curvature of the free-energy concentration plot at a given composition. $\varkappa$ is the gradient-energy coefficient and is positive for systems exhibiting clustering (positive heat of mixing). The value of $(\partial^2 F/\partial c^2)$ is negative within the spinodal region and corresponds to a situation where the solution is unstable to the smallest compositional fluctuation. The amplification function, equation (4), contains the essence of spinodal decomposition. $R(\beta)$ increases from zero with increasing β, passes through a maximum at

$$\beta = \beta_{max.} = \left(\frac{-DN_v}{4M\varkappa}\right)^{\frac{1}{2}}. \; R(\beta) = 0 \text{ at } \beta = \beta_c = \left(\frac{-DN_v}{2M\varkappa}\right)^{\frac{1}{2}}$$

being thereafter negative at values of $\beta > \beta_c$.

Thus, those Fourier amplitudes describing the composition will increase for $0 < \beta < \beta_c$, the Fourier amplitude corresponding to $\beta_{max.}$ growing at the fastest rate, while those Fourier amplitudes with $\beta > \beta_c$ will decrease with time.

X-rays are scattered by fluctuations in electron density, and thus can be used to examine variations in composition. It was recognized by Rundman and Hilliard[4] that a formal correspondence exists between the Fourier amplitudes associated with compositional fluctuations and the amplitude of the X-rays scattered to a point, **s**, in reciprocal space: the latter is given by the usual formula,

$$F(\mathbf{s}, t) = \int_v \rho(\mathbf{r}, t) \exp [-2\pi i \mathbf{s}.\mathbf{r}]\, d\mathbf{r} \qquad \ldots (6)$$

where $\mathbf{s} = \beta/2\pi$ and $\rho(\mathbf{r}, t)$ is the electron density at **r** at time t. Writing

$$\rho(\mathbf{r}, t) = \rho_0 + (f_B - f_A)\,[c(\mathbf{r}, t) - c(\mathbf{r}, 0)] \ldots (7)$$

where f_A and f_B are the scattering factors for the A and B components, and ρ_0 is the average electron density for the system, the amplitude of the scattered X-rays is, neglecting the (000) peak

$$F(\mathbf{s}, t) = (f_B - f_A) \int_v [c(\mathbf{r}, t) - c(\mathbf{r}, 0)] \exp (-2\pi i \mathbf{s}.\mathbf{r}) d\mathbf{r}$$
$$= (f_B - f_A)\, A(\mathbf{s}, t) \qquad \ldots (8)$$

The intensity of the scattered X-rays is then given by

$$F^2(\beta, t) = F^2(\beta, 0) \exp [2R(\beta)\, t] \qquad \ldots (9)$$

and the amplification factor is thus obtained from equation (9)

$$R(\beta) = (1/2) \ln [F^2(\beta, t)/F^2(\beta, 0)]\, t^{-1} = (1/2)\alpha\, t^{-1} \qquad \ldots (10)$$

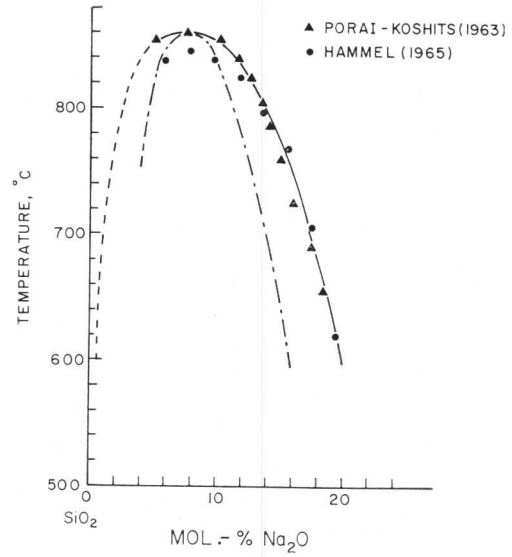

Fig. 1 Metastable miscibility gap in the Na_2O–SiO_2 vitreous system.[5,6] Spinodal calculated by the method of Cook and Hilliard.[7]

i.e., $R(\beta)$ may be obtained as 1/2 the slope of α plotted vs. time and α is simply the natural logarithm of the normalized X-ray intensity at a given angle.

In the present research, the two-component glass Na_2O–SiO_2 is considered to be elastically isotropic. It is known that this system shows complete miscibility at high temperatures, but has a miscibility gap at low temperatures[5,6] (Fig. 1). A range of compositions annealed over a range of temperatures was examined. The breakdown of the initial solution was examined using the technique of small-angle X-ray scattering after the glass had been brought to within the miscibility gap. The X-ray spectra are evaluated after the method of Rundman and Hilliard,[4] and hence it is determined that spinodal decomposition is operating. An interdiffusion coefficient is obtained from the data, and this value agrees well with literature values of the oxygen self-diffusion coefficient in silica-glass systems.

Experimental

Calculated amounts of analytic reagent grade Na_2CO_3 and $SiO_2.nH_2O$ were combined. As_2O_3 (0·5 wt.-%) was added as a refining agent. The batch was mixed until homogeneous and then transferred to a 50-cm^3 alumina crucible and presintered at 1000° C. After cooling, the sintered batch was transferred to a fresh 50-cm^3 alumina crucible, which was inserted into a carbon susceptor. Melting was accomplished with a 15-kW induction furnace under an argon atmosphere. For a given composition, the maximum temperature during melting exceeded the solidus by at least 100 degC, the melt being maintained at this temperature for 1·5 h. The melt was then poured into a shallow carbon mould, pressed by a carbon block, and shaped into a sample 40 × 40 × 5 mm. The sample was immediately transferred to a furnace at a temperature of 150 degC below the annealing point of the glass and then furnace-cooled. This procedure was employed to avoid build-up of excessive strain which could result in cracking and also to avoid appreciable phase separation. Spectroanalysis showed that the impurity content was < 0·2 wt.-%. The Na_2O content was determined by flame-photometry (Table I).

TABLE I

Glass No.	Mol.-% SiO_2	Mol.-% Na_2O	Impurities (Al_2O_3, Fe_2O_3, As_2O_3)
1	88·1	11·7	0·2
2	86·8	13·0	0·2
3	84·3 (4)	15·5	0·1 (6)
4	82·3 (8)	17·5	0·1 (2)

For X-ray small-angle scattering studies, slices 1 × 40 × 5 mm were sectioned, using a diamond saw. The slices were then polished to obtain the optimum thickness (0·15 mm). Preliminary experiments showed that the surface condition influences the X-ray scattering intensity at the lowest angles; the following polishing steps were required: (1) Abrasive papers, grit 240 (~ 45 μm), 320 (~ 32 μm), 400 (~ 25 μm), 600 (~ 15 μm); (2) diamond powder, 6 μm; (3) alumina powder, 0·3 μm, 0·05 μm. Polishing with abrasive paper 600, diamond 6 μm, and alumina 0·3 μm, 0·05 μm was repeated after every heat-treatment to remove the surface material that formed during the heat-treatment.

Following each heat-treatment, an X-ray small-angle scattering scan was carried out with a unit employing Kratky collimation with automatic step-scanning. A G.E. high-intensity X-ray tube was operated at 34 kV at 40 mA with CuK_α radiation being obtained by nickel filtration; pulse-height analysis and a proportional counter were incorporated. Entrance and exit slit apertures were adjusted to satisfy the infinite slit-height condition.[8]

The scattered intensity was measured for 200 or 1000 sec depending upon intensity. Parasitic and background scattering were subtracted. The intensity so obtained was corrected for slit-width[9] and slit height[10] using a computer method. In the programme, calculation of $\tilde{I}(2\theta)^3$, $\tilde{I}(2\theta)\ I(2\theta)^4$, and $I(2\theta)^2$, were employed to determine the Invariant[11] and to carry out a Porod's Law analysis,[12] where $\tilde{I}$ and I are the scattered intensities before and after slit-height correction, respectively, and 2θ is the scattering angle.

Results

The scattering curves with logarithmic ordinate are shown in Fig. 2 for a 13·0 mol.-% Na_2O–86·8 mol.-% SiO_2 glass, isothermally heat-treated at 580° C for progressively longer times. The logarithmic scale was chosen since, according to the theory of the early stage of spinodal decomposition, the intensity at a given angle is expected to change exponentially with time. The scattering curves for all glasses studied showed similar trends; the initially smooth-falling curve gradually evolves a maximum which sharpens with the time of heat-treatment.

Fig. 2 shows that the wave number associated with the maximum value of the Fourier amplitudes shifts towards smaller angle (smaller wave number) and the maximum of the amplification factor (which is proportional to the maximum difference of the intensity in log scale in unit time) decreases with time of heat-treatment. In addition the cross-over point for the two successive curves shifts to lower angles. These shifts to lower angles are not predicted by the original theory and thus if spinodal decomposition is in fact occurring in the present case, it departs from the strictly ideal behaviour predicted by equation (4). In fact, it has been shown by de Fontaine[13] that for a system having a composition not at the centre of the miscibility gap, this behaviour, i.e. the shift to lower angles, is expected.

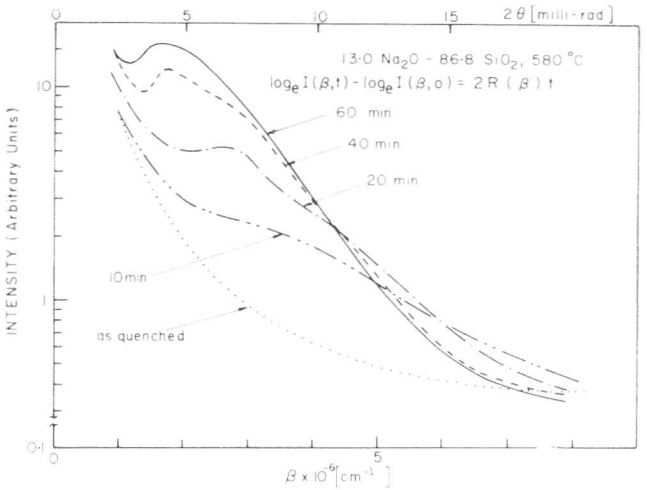

Fig. 2 Log X-ray intensity, I, vs. β for 13·0% Na_2O–86·8% SiO_2 glass after various times of heat-treatment at 580° C.

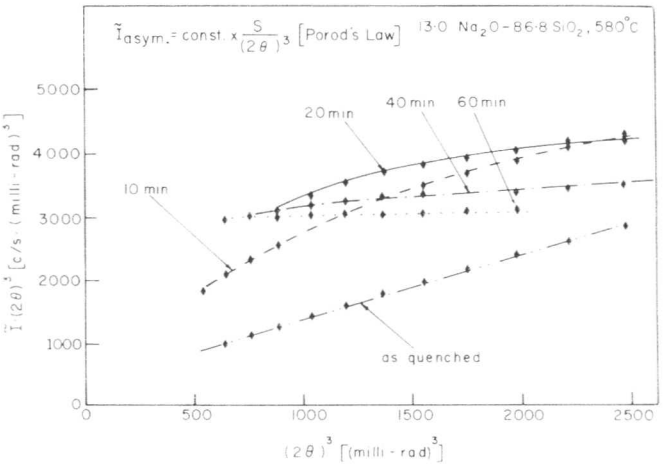

Fig. 3 $\tilde{I}\ (2\theta)^3$ vs. $(2\theta)^3$ for 13·0% Na_2O–86·8% SiO_2 glass after various heat-treatments at 580° C: Porod's Law.

The degree of interfacial diffuseness associated with a growing inhomogeneity is important in characterizing the process. This may be investigated by the method of Porod.

According to Porod[12] $\tilde{I}(2\theta)^3$ is a constant if there is a sharp interface between the two phases, and is proportional to the interface area. Consequently if $\tilde{I}(2\theta)^3$ is plotted against $(2\theta)^3$, a constant value should be obtained if the interface is sharp. A sharp interface is normally associated with a particle formed by nucleation and growth. In Fig. 3 it is seen that Porod's law is not satisfied initially, $\tilde{I}(2\theta)^3$ being a monotonically increasing function. After 60 min heat-treatment at 580° C, however, $\tilde{I}(2\theta)^3$ becomes nearly constant indicating that the interface is virtually sharp, i.e. that the system departs appreciably from conditions where spinodal decomposition is expected. Although at present there is no quantitative theory concerning X-ray scattering associated with a diffuse interface, this result indicates qualitatively how the concentration gradient at the interface is sharpening.

From the results of Figs. 2 and 3 it can be concluded that only the first few curves correspond to the early stage of phase separation; i.e. the most ideal conditions in which to investigate spinodal decomposition. This is also confirmed by an

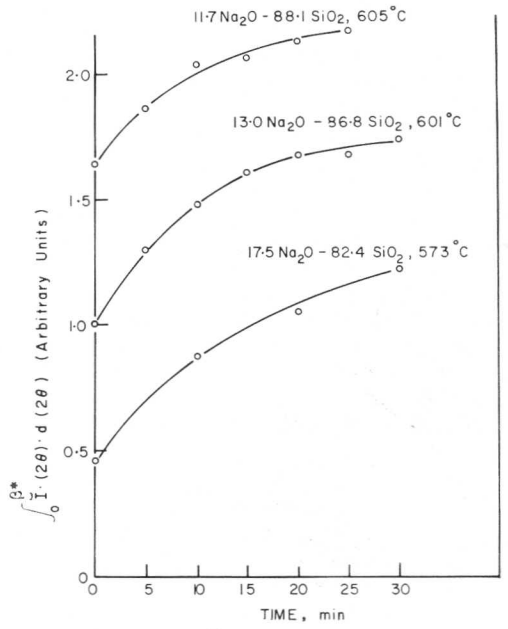

Fig. 4 The Invariant $\int_0^{\beta^*} \tilde{I}\ (2\theta)\ .\ d(2\theta)$ *vs.* t *for various compositions and annealing temperatures.*

evaluation of the Invariant, $\int_0^{\infty} \tilde{I}\ (2\theta).d\ (2\theta)$, which is proportional to the amount of phase separation.[11] This function is plotted in Fig. 4. In evaluating the Invariant, an upper limit was set at $\beta^* = 8 \times 10^{-6}$ cm^{-1} so that fluctuations having wave numbers greater than this cut-off value are not considered. The increasing value of the Invariant points to the development with time of concentration inhomogeneities within the system. Thus it can be concluded that coarsening is not significant in the early stage of the process.

The first two sets of X-ray scattering curves after heat-treatment at various temperatures are shown in Fig. 5 on a logarithmic scale for a 13·0 mol.-% Na_2O–86·8 mol.-% SiO_2 glass.

The wave number corresponding to the maximum amplification, $\beta_{max.} = 2\pi/\lambda_{max.}$ shifts toward smaller values as the heat-treatment temperature increases. This is predicted by the early-stage theory. Using these two sets of curves, an analysis for the interdiffusion coefficient was made following Rundman and Hilliard's technique.[4] The interdiffusion coefficient for 13·0 mol.-% Na_2O–86·8 mol.-% SiO_2 glass is shown in Table II. Also shown in Table II are the values of the interdiffusion coefficient obtained in the same way for a 15·5 mol.-% Na_2O glass. These values agree within an order of magnitude with the diffusion coefficient of oxygen in silicate glasses[14–16] at the same temperature, thus suggesting that the oxygen is the rate-controlling diffusing species in the phase separation of this system. This fact was also pointed out by Weyl and Marboe.[17]

Finally the earliest stage of phase separation was investigated in some detail. The results (Fig. 6) show that there is an exponential increase of the X-ray intensity at a given angle with time. This is strictly in accord with the theory of spinodal decomposition. However, owing to the extremely low intensity consequent on there being almost no phase separation, the calculation of an amplification function of the predicted form could not be obtained.

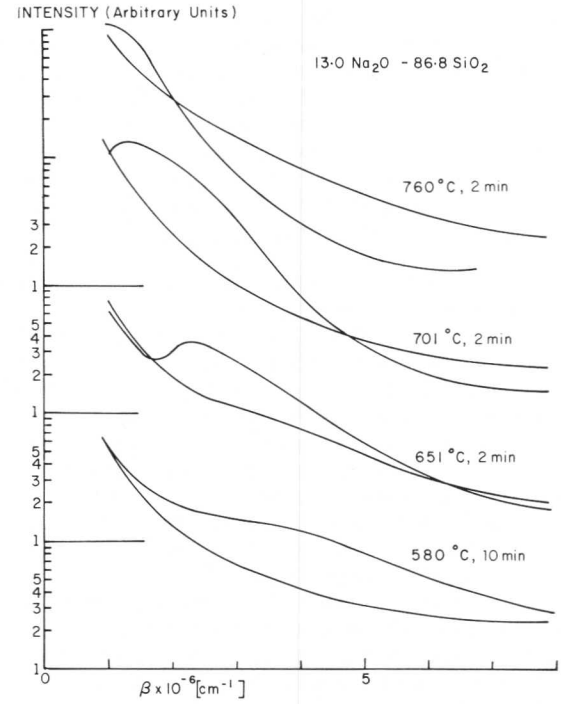

Fig. 5 Log I *vs.* β *for 13·0% Na_2O–86·8% SiO_2 glass after various heat-treatments.*

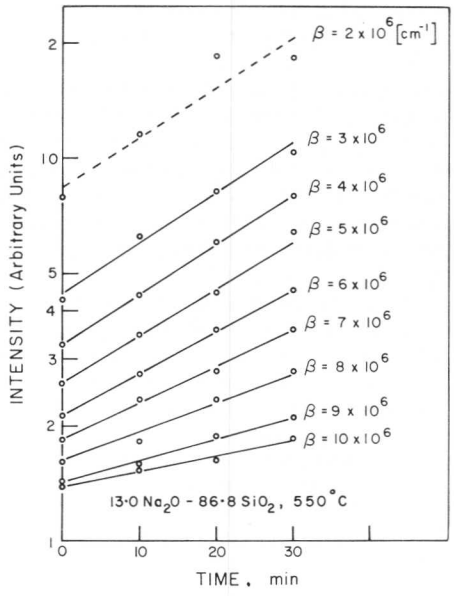

Fig. 6 Log I *vs.* t *for 13·0% Na_2O–86·8% SiO_2 glass after heat-treating at 550° C for various values of* β.

TABLE II

13·0 % Na_2O–86·8% SiO_2		15·5% Na_2O–84·3% SiO_2	
Temp.,°C	D, cm² . sec⁻¹	°C	D, cm² . sec⁻¹
540	$-1{\cdot}0 \times 10^{-17}$	525	$-7{\cdot}0 \times 10^{-18}$
560	$-2{\cdot}0 \times 10^{-17}$	545	$-2{\cdot}0 \times 10^{-17}$
580	$-1{\cdot}0 \times 10^{-16}$	565	$-3{\cdot}0 \times 10^{-17}$
601	$-3{\cdot}0 \times 10^{-16}$	595	$-1{\cdot}5 \times 10^{-16}$
651	$-1{\cdot}0 \times 10^{-15}$		

Discussion

The low-angle X-ray scattering spectrum as shown in Fig. 2 does qualitatively satisfy the requirements stipulated for a system decomposing spinodally; there is preferential development in X-ray intensity at wavelengths narrowly clustered around a given $\lambda = \lambda_{max}$, so that composition fluctuations of these wavelengths must increase preferentially. In addition, owing to the initial presence of quenched inhomogeneities, there is a decay of the Fourier amplitudes for values of β greater than the critical value, β_c, as expected from the theory. It is obvious from Fig. 2 that the value of β which corresponds to the maximum rate of growth is associated with $\lambda \simeq 300$ Å.

From the treatment of Rundman and Hilliard,[4] it would be expected that equation (4) should be satisfied and that a plot of $R(\beta)$ vs. β should yield not only $\beta_{max.}$, but also β_c. However, an examination of the scattering curves of Fig. 2 shows that the crossover point which corresponds to β_c, is shifting as a function of time. This deviation from what might be thought to be " ideal behaviour " has been discussed extensively by de Fontaine,[13] who shows theoretically that there should indeed be a shift of the maximum with time, and an attendant displacement of the crossover point, when the composition of solution is not at the centre of the miscibility gap. Fig. 1 shows that this corresponds to the present case.

The Porod-law analysis also points to the operation of a spinodal mode since the slope of the plot of $\tilde{I}(2\theta)^3$ plotted vs. $(2\theta)^3$ (Fig. 3) decreases with time to zero, indicating a sharpening of an initially diffuse interface. The Invariant function (Fig. 4) indicates that the solution is becoming depleted with time, pointing to the fact that coarsening, at least at early times, is not an important part of the processes being observed here.

The X-ray-scattering Fourier amplitudes of a sample with a very small amount of phase separation indicate that $\ln I$ vs. t is linear (Fig. 6). This is strong evidence for spinodal decomposition. However, there is some deviation from linearity at larger values of α, and, in addition, the 1/2 slope does not clearly decrease as expected from theory. This we attribute to experimental limitations when there is small phase separation in the sample. The inherent inaccuracies in the measurements of the X-ray intensity changes are expected to be most serious at this early stage. In addition these inaccuracies are magnified by the slit-height correction, which is most inaccurate at small angles. (Notice that we do not expect to see negative values of $R(\beta)$ since the Fourier amplitudes of a well-quenched sample at large values of β are essentially zero.) Unfortunately, owing to experimental limitations, we were unable to demonstrate the maximum in $R(\beta)$ in almost homogeneous specimens as predicted in the theory.

Conclusions

In this work it has been demonstrated that: (1) the X-ray spectra are changing in a way that indicates the selective development of composition fluctuations within a narrow range of wavelengths; (2) the interface is becoming less diffuse with time; and (3) coarsening is not an important feature of the process, at least in the early stage.

On a more quantitative level, the value of the diffusivity, as determined from the data of Fig. 5, is of the right order of magnitude—that of oxygen in soda-lime-silica glass. Data are lacking for diffusion of oxygen in the glass under consideration here, but it is clear that diffusion of the anion is the rate-controlling step in the process of phase separation under consideration.

The gradient energy coefficient, $\varkappa$, was not determined because of lack of sufficient thermodynamic data.

Acknowledgement

This research was supported by the Advanced Research Projects Agency of the United States Department of Defense.

References

1. J. W. Cahn and R. J. Charles, *J. Phys. Chem. Glasses*, 1965, **6**, 181.
2. A. J. Ardell, R. B. Nicholson, and J. D. Eshelby, *Acta Met.*, 1966, **14**, 1295.
3. J. W. Cahn, *J. Chem. Physics*, 1965, **42**, 93.
4. K. B. Rundman and J. E. Hilliard, *Acta Met.*, 1967, **15**, 1025.
5. N. S. Andreev, D. A. Gogarov, E. A. Porai-Koshits, and Yu. G. Sokolov, " Structure of Glass ", Vol. 3, p. 47. **1964:** New York (Consultants Bureau).
6. J. J. Hammel, private communication.
7. H. E. Cook and J. E. Hilliard, *Trans. Met. Soc. A.I.M.E.*, 1965, **233**, 142.
8. O. Kratky, G. Porod, and Z. Skala, *Acta Phys. Austriaca*, 1960, **13**, 76.
9. Ref. 8, modified by A. Bienenstock, private communication.
10. P. W. Schmidt, *Acta Cryst.*, 1965, **19**, 938.
11. A. Guinier and G. Fournet, " Small-Angle Scattering of X-Rays". **1955:** New York and London (John Wiley).
12. A. Guinier, " X-Ray Diffraction ". **1963:** San Francisco (Freeman).
13. D. de Fontaine, Ph.D. Thesis, Northwestern Univ., **1967.**
14. T. B. King and P. J. Koros, " Kinetics of High-Temperature Processes ", p. 30. **1959:** New York and London (John Wiley).
15. W. D. Kingery and J. A. Lecron, *J. Phys. Chem. Glasses*, 1960, **1**, 87.
16. W. C. Hagel and J. D. Mackenzie, *ibid.*, 1964, **5**, 113.
17. W. A. Weyl and E. C. Marboe, " The Constitution of Glasses ", Vol. II, Pt. 1, p. 712. **1964:** New York and London (John Wiley).

A Study of Precipitation in a Cu–16% Ni–10% Co "Side-Band" Alloy

V. A. Phillips

The alloy, designed to have the same phase compositions as Cunico 2 after precipitation at 650° C but only ~ 10 vol.-% of the magnetic phase, contained 16·6 wt.-% nickel, 10·5 wt.-% cobalt, balance copper. After solution-treatment at 1100° C, foil samples aged for up to 1 week at 650° C were studied by microhardness, X-ray diffraction, and transmission electron microscopy. A single-peak ageing curve was observed, the diamond pyramid hardness increasing from 98 to 195 kg/mm² at peak after 5 h ageing. Although only X-ray lines from the matrix were detected in the solution-treated condition, fine particles < 20 Å in width were seen by electron microscopy. Faint side-bands were detected after ageing for 1 min, which became strong after ageing for 15 min–5 h and disappeared after ageing for 24 h–1 week. Precipitation apparently continued up to peak ageing. In the overaged condition, two f.c.c. phases were detected; the lattice parameters after ageing for 1 week were 3·598 Å (matrix) and 3·541 ± 0·002 Å (precipitate) giving a misfit of 1·57%. Electron microscopy showed progressive growth of particles on ageing with loss of coherency at 250 ± 50 Å width. After ageing for 5 h, the particles were cubical with edges parallel to ⟨001⟩ directions and highly aligned in rows parallel to cube directions. On gross overageing the particle network was destroyed by impingement, coalescence, and spheroidization; discontinuous precipitation became appreciable. Interpretations of the X-ray side-bands are discussed.

There is a great deal of interest in coherent precipitation in systems such as Cu–Co[1] and Ni–Al[2,3] in which precipitation appears to occur by classical nucleation and growth. Coherent precipitation occurs in another important group of alloys: the so-called " side-band alloys " (see reviews[4,5]) which include the precipitation-hardened magnetic alloys Cunife and Cunico. The name refers to the fact that the principal reflections in X-ray powder patterns made from these alloys are flanked on either side by a satellite or side-band, usually diffuse in nature. By analogy with similar phenomena in optical gratings and radio-wave theory, side-bands are usually ascribed to a periodic modulation of the lattice having a repeat interval much larger than the unit cell. Typically the side-band alloys exist at high temperatures as a single f.c.c. phase, but show a miscibility gap at low temperatures.

Manuscript received 22 February 1968. V. A. Phillips, D.Eng., B.Sc., A.R.S.M., F.I.M., is in the Metallurgy and Ceramics Laboratory, General Electric Research and Development Center, Schenectady, N.Y., U.S.A.

A number of models of "clustering" in solid solutions have been proposed to explain side-band formation[4–7] and a general theory of diffraction from one-dimensional modulated structures developed.[6] There is controversy over the question of whether decomposition occurs spinodally in the side-band alloys or by classical nucleation and growth. Spinodal decomposition appears to offer a ready explanation of the periodic structures observed in side-band alloys.

The precipitation sequence in a commercial Cunico 1 alloy containing 21% Ni, 29% Co, 50% Cu, after quenching from high temperature, appears to be:[8,9]

Supersaturated solid solution → pre-precipitation (characterized by side-bands) → two tetragonal phases (precipitate plates and depleted matrix, both coherent with parent matrix on {001}) → two equilibrium f.c.c. phases.

The structure of Cunico 1 was studied by Tufton[10] using transmission electron microscopy; he concluded that the single-phase f.c.c. structure obtained on solution-treatment decomposed on ageing at 600–900° C to give rods on {001} matrix planes, in disagreement with the plate morphology inferred by Geisler and Newkirk.[8] He suggested that decomposition occurred spinodally. The magnetic properties of the Cu–Ni–Co alloys have been reviewed by Bozorth.[11]

It was thought that a dilute alloy would offer an advantage over Cunico in that the smaller volume fraction of precipitate would reduce the degree of connectivity and enable particle alignment effects to be identified. By studying the early stages of ageing, it should be possible to distinguish alignment due to spinodal decomposition from that now known[1–3] to be developed by selective growth. It was hoped that the use of X-ray diffraction combined with transmission electron microscopy would enable the structural features responsible for side-bands to be elucidated.

Experimental Details

The alloy composition chosen lay on a tie-line drawn through the Cunico 2 composition (nominally 41 wt.-% Co, 24% Ni, 35% Cu) to intercept the solvus for 650° C,[12] and thus should give the same phase compositions as Cunico 2 after precipitation at 650° C. The solubility isotherms[13] indicated that the alloy would be single phase above ~ 900° C, and that the alloy series across the chosen tie-line would be completely miscible at high temperature in the solid state and show a miscibility gap at lower temperatures. Thus, the alloy is of the spinodal type.

The alloy was vacuum induction-melted in an alumina crucible from 99·999% oxygen-free copper, 99·98% nickel, and 99·58% purity electrolytic cobalt in which the principal

impurity was 0·39% nickel. It was solidified and remelted several times to remove gas, then cast into a graphite mould in vacuum giving a 1·2-in.-sq. ingot. Chemical analysis showed 16·6 wt.-% (17·6 at.-%) nickel and 10·5 wt.-% (11·1 at.-%) cobalt. The ingot was homogenized for 48 h at 1050° C in argon, cooling in a cooling chamber. A $\frac{3}{8}$-in. slice was cold rolled 80%, solution-treated for 2 h at 1000° C while sealed in quartz in vacuum, and quenched into cold water using a device to snap off the nose of the tube. Finally, it was cold rolled 94% to 0·005 in. thickness.

After solution-treating at 1000° C sealed in vacuum and quenching into iced brine, 40 Å-dia. particles were visible in the electron microscope. Solution-treatment at 1100° C for 1 h was therefore adopted to increase the initial quenching rate and to enable the particle size to be kept down to ~ 20 Å in the quenched material.

Strips were aged for up to 1 week at 650 ± 2° C and then withdrawn into the cooling zone of the vacuum furnace; the initial cooling rate was estimated to be ~ 50 degC/sec. The hardness was determined in a Kentron microhardness tester on a lightly electropolished spot on the strip surface using a 300-g load and a diamond pyramid indenter. Longitudinal sections of all the strips were etched and examined in the light microscope.

Discs of 2·3 mm dia. punched from the strips were electro-thinned by a Disa jet technique[14] for electron-microscope examination at 100 kV. The electrolyte consisted of equal parts of orthophosphoric acid (sp. gr. 1·70) and water at 95 V. In some cases an alternative electrolyte, consisting of 5 vol.-% perchloric acid (70%) and 95% glacial acetic acid, was used at 150 V. Both single-tilt and double-tilt Valdrè[15] holders were employed.

Pieces of all the strips, chemically thinned to 0·001 in., were examined in forward reflection in a Guinier–Jagodzinski double-cylinder focusing X-ray camera using monochromated CuK_α radiation. The sample was oscillated during exposure. Calibration lines were provided by tungsten powder of known parameter placed on one edge of the sample. A few samples were also examined in a 114-mm-dia. Debye–Scherrer camera using CoK_α radiation and 16 h exposure. Side-bands were not detected by this technique. The measured lattice parameters were accurate to ± 0·002 Å, but the side-bands could only be measured to lesser accuracy on account of their diffuse nature.

Results

Hardness tests gave a single-peak ageing curve. The average hardness increased progressively from 98 kg/mm² as solution-treated to 195 kg/mm² peak after 5 h ageing at 650° C, and then decreased to 143 kg/mm² after 1 week (Fig. 1).

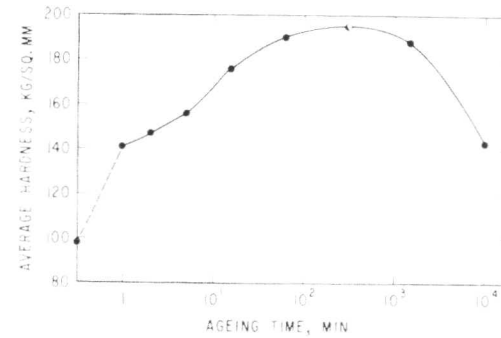

Fig. 1 Variation of average hardness with the logarithm of the ageing time at 650° C.

In the solution-treated condition, the focusing camera revealed only matrix lines corresponding to an f.c.c. lattice with $a_0 = 3{\cdot}591$ Å, with no evidence of side-bands. Side-bands were detected after ageing at 650° C for periods of 1 min–5 h (corresponding to peak ageing) but were absent after overageing for 24 h or 1 week. The lattice parameter increased gradually on ageing, attaining an average value of 3·598 Å after 1 week.

A separate f.c.c. precipitate phase was first detected in the sample aged 24 h at 650° C. The mismatch increased to 1·57 ± 0·11% average after ageing for 1 week, corresponding to lattice parameters of 3·598 Å (matrix) and 3·541 Å (precipitate), compared with the expected[12] values of 3·592 and 3·525 Å, respectively. No new lines corresponding to a tetragonal stage appeared between the side-band stage and the formation of the f.c.c. phases, although these would be expected from the work of Biedermann and Kneller.[9]

To investigate whether the volume fraction of the equilibrium phases (formed as discontinuous precipitate nodules) became large enough to contribute to the diffraction patterns, estimates were made by lineal analysis on metallographic sections which showed 0·1, 0·8, 1·6, and 6·5 vol.-% after ageing times of 1 h, 5 h, 24 h, and 1 week, respectively. Since only ~ $\frac{1}{10}$ of this would be precipitate, it is unlikely to be detectable in any of the diffraction patterns. The matrix phase would be barely detectable after 24 h, but should make some diffraction contribution after 1 week. The lines apparently coincided with those from the rest of the matrix.

Side-bands were visible on either side of the fundamental lines 111, 200, 220, 311, and 222 of the original f.c.c. lattice. The side-bands were very faint after 1–5 min ageing at 650° C, strong after 15 min ageing (Fig. 2), remained strong with further increase in ageing time up to 5 h, and were not detectable after 24 h ageing. No second-order peaks were observed. The sidebands on the two sides of a fundamental line often differed from one another in intensity, in one case from arc to arc along the same diffraction line. This is taken to indicate a grain-to-grain variation in diffraction behaviour. Arcing and diffuseness of the matrix lines, associated with moderately coarse grains and preferred orientation, resulted in less than ideal X-ray patterns. However, the peak positions of the side-bands for the 200 and 111 reflections were measured where possible. Their displacement Δd from the main line tended to decrease on ageing. The first, i.e. higher d value, side-band tended to approach the main line on continued ageing, while the second side-band approached the parameter at which the f.c.c. precipitate appeared on overageing.

The light microscope showed evidence of abnormal grain-boundary structures in the etched microsections. A few of the grain boundaries in the solution-treated sample were abnormally thick and one or two showed slight discontinuous precipitation. The number of grain boundaries affected and the size of the precipitate nodules increased on ageing. Most boundaries showed discontinuous precipitation in the peak-aged condition; this led to intergranular cracking when strips aged for 1 h or more were slightly deformed.

The electron micrographs obtained are illustrated in Figs. 3 and 4. Even quenching from 1100° C into iced brine at an initial rate of ~ 8000 degC.sec^{-1} failed to suppress precipitation and resulted in an average particle size of ~ 20 Å dia. (Fig. 3(*a*)). The particle size gradually increased with increase in ageing time at 650° C (Figs. 3 and 4), being ~ 50 Å after 5 min

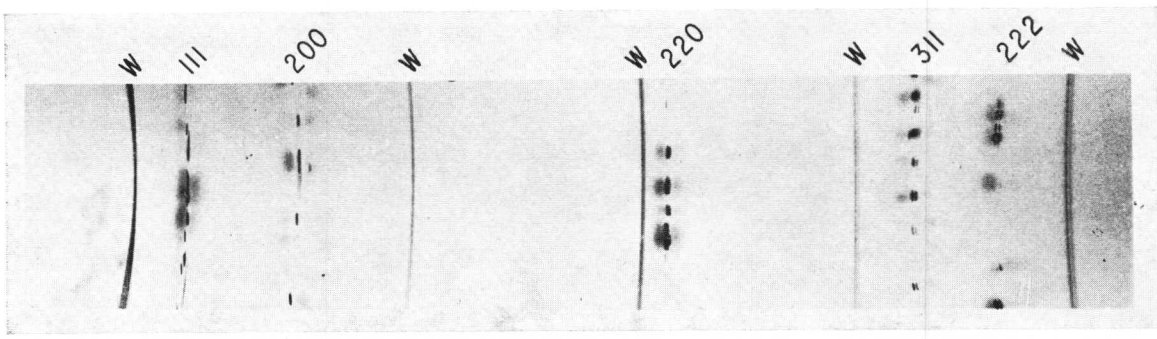

Fig. 2 X-ray diffraction pattern of sample aged 15 min at 650° C, showing side-bands.

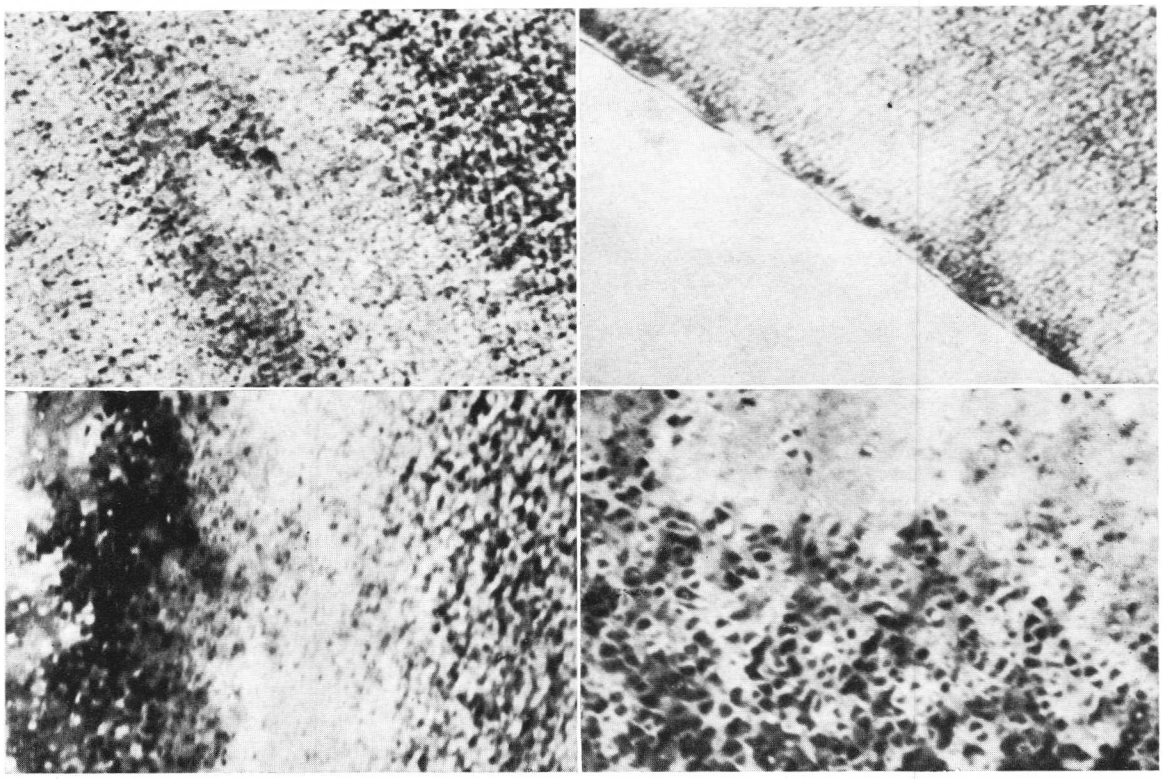

Fig. 3 Electron micrographs showing the effect of ageing at 650° C: (a) no ageing; (b) aged 2 min; (c) aged 5 min; (d) aged 1 h. Note growth of coherent precipitates, incipient discontinuous precipitation at grain boundary in (b), and strain fields at particles in (d). × 200,000.

(Fig. 3(*c*)), 150 Å after 5 h (Fig. 4(*a*)), corresponding to peak ageing, and becoming much coarser on overageing (Figs. 4(*b*)–(*d*).

A grain boundary on a sample aged for 2 min had an irregular wave-like shape and appeared to show a denuded zone of irregular thickness, presumably due to incipient discontinuous precipitation (Fig. 3 (*b*)). After ageing for 1 week general precipitation was typically observed on one side of a grain boundary and discontinuous precipitation on the other (Fig. 4(*c*)). Although there was relatively little change in microstructure during the first 2 min ageing, the hardness increased considerably from 98 to 148 kg/mm^2 (Fig. 1).

In the sample aged for 1 h (Fig. 3(*d*)), it was seen that the contrast at a particle consisted of two dark lobes separated by a plane of no contrast. In other regions, the plane of no contrast was identified as being parallel to the principal diffracting plane. It was uncertain whether the particles were spheres or cubes with rounded corners but it was concluded that the particles were coherent and were visible by strain-field contrast.[2,16–18] This conclusion is supported by the fact that ring patterns could not be obtained from the particles by selected-area diffraction, and that in the overaged samples electron diffraction indicated that the particles had the same orientation as the matrix.

The particles produced by ageing for 5 h, corresponding to peak hardness, were cubical with edges parallel to cube matrix directions as apparent in (001) foils (Fig. 4(*a*)). The contrast observed indicated that the particles were still coherent. A marked tendency for the particles to be aligned in rows parallel to cube matrix directions was now apparent. The distribution of row spacings was most easily measured in an (011)-oriented foil. The measured distribution after 5 h ageing had a rather broad peak centred about 250 Å.

After 24 h ageing, the smaller precipitates were generally

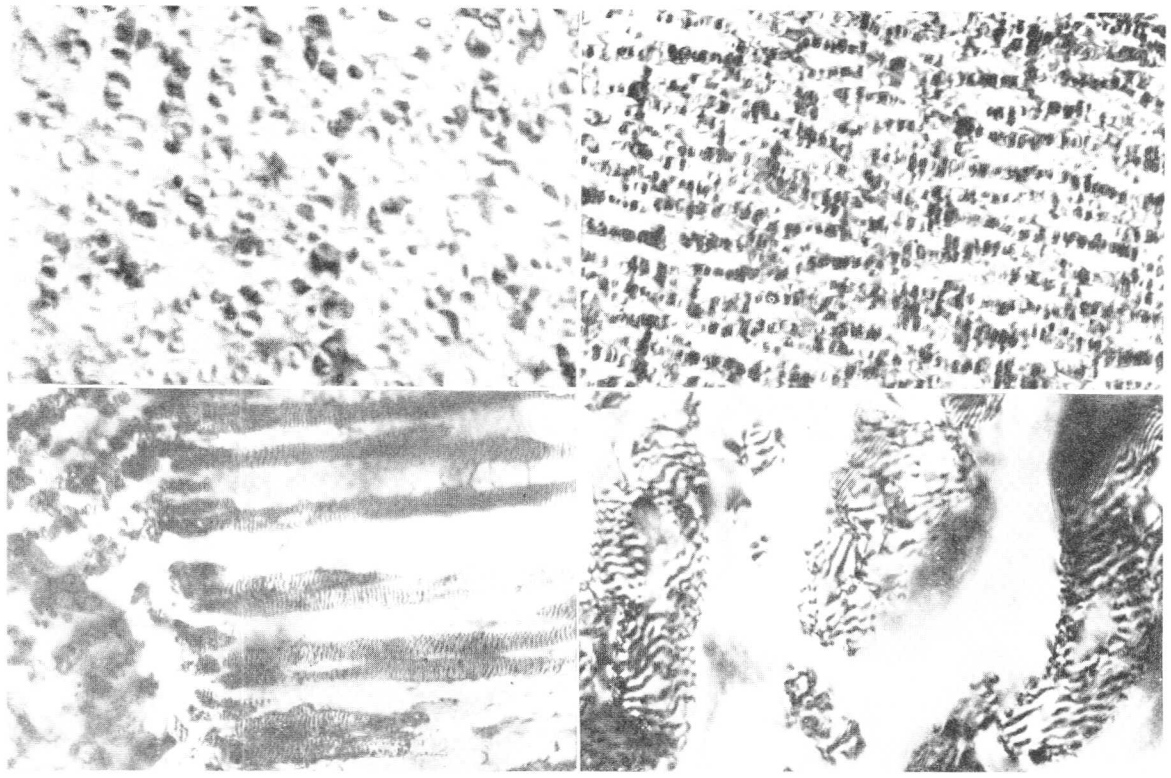

Fig. 4(a) Aged 5 h at 650° C. The foil is a few degrees off (001) *and the micrograph edges are parallel to* ⟨001⟩. *Showing cubical precipitates tending to align in rows.* × 200,000. *(b) Aged 24 h at 650° C. The foil plane is* (011) *and the long edge of the micrograph is parallel to* [00$\bar{1}$]. *Showing pronounced alignment of precipitates.* × 80,000. *(c) Aged 1 week at 650° C. Showing discontinuous precipitates (striated) adjoining a grain boundary. The orientation in the discontinuous region is* (112). × 40,000. *(d) Aged 1 week at 650° C. Showing general precipitation in a* (112) *foil. The precipitates show moiré fringes.* × 125,000

still coherent (Fig. 4(*b*)) but there was evidence of loss of coherency of the larger particles in some areas. Alignment of particles in rows in cube directions was marked leading to a remarkably regular 3-dimensional array. The distribution of row spacings, measured normal to the rows in an (011) foil area including Fig. 4(*b*), peaked at ~ 350 Å. As noted earlier, X-ray side-bands were no longer observed at this ageing time.

Considerable coalescence and some spheroidization of the particle rows had occurred after ageing for 1 week at 650° C, leading to a wide range of general precipitate morphologies (Figs. 4(*c*) and (*d*)). The particles had evidently lost coherency judged by criteria established previously,[1] since pronounced moiré fringes were observed at the particles and strain fields were now absent. Two of the sets of moiré fringes apparent in Fig. 4(*d*) were in the correct directions for {111} and {511} types. Their spacings were measured and agreed within experimental accuracy with the values of 130 and 44 Å calculated for parallel-type moiré patterns from the measured X-ray lattice parameters.

Selected-area diffraction on the discontinuous precipitate region in Fig. 4(*c*) indicated that the precipitates had the same orientation as the matrix and the positions of the reflections agreed with the measured X-ray lattice parameters. The particles were elongated parallel to a ⟨111⟩ direction; fringes were seen parallel to a ⟨110⟩ direction in this (112)-oriented region and could be interfacial dislocations or a {111} parallel moiré pattern. The average fringe spacings measured at three particles were 141, 150, and 160 Å, compared with 136 Å calculated for a {111} parallel moiré pattern from the X-ray lattice parameters, or 165 Å calculated for the spacing of an array of unit edge dislocations needed to accommodate the 1·57% mismatch. Contrast experiments would be necessary to make a distinction.

Discussion

Contrary to what might have been expected from previous work[8–10] on Cunico 1, the general precipitate shape after ageing for 5–24 h at 650° C was cubical. It was not possible to distinguish between cubes and spheres at shorter ageing times. No particle alignment in rows parallel to ⟨001⟩ matrix directions was detected at the beginning of ageing, where it would be expected if decomposition occurred spinodally, although a number of {110} foils were examined. While this might be ascribed to difficulties of observation associated with the high particle density, it seems more likely that selective growth was needed to develop alignment as observed in Cu–Co[1] and Ni–Al[2,3] alloys.

Pronounced alignment of particles in rows parallel to ⟨001⟩ directions was apparent in the peak-aged and lightly overaged conditions, corresponding to a 3-dimensional array with remarkably uniform spacings. Coalescence, loss of coherence, and spheroidization leading to the formation of relatively coarse, isolated precipitate particles occurred on prolonged overageing. Thus, the structure apparently changed from a random array of isolated particles to a 3-dimensional interpenetrating network and back to a random array of isolated particles. Since the initial solid solution gave sharp lines and the lattice parameter gradually moved towards the final

matrix parameter on ageing, it was concluded that precipitation continued up to a late stage in ageing, possibly up to the point at which the f.c.c. precipitate lines were detected.

The particle width at which loss of coherency occurred, judged by the largest coherent and the smallest incoherent particles observed after ageing for 1 week at 650° C (mismatch 1·57%), was 250 ± 50 Å. On the argument that a single dislocation of unit [110] Burgers vector ($b = 2{\cdot}54$ Å) every 64 planes would just accommodate a mismatch of 1·57%, loss of coherency might be expected to occur at a particle width of ~ 160 Å, which is somewhat less than the 250 ± 50 Å width observed.

The onset of overageing is attributed to the progressive loss of coherency, general coarsening of the structure, and increase in particle spacing. This means that the Orowan stress for looping between the particles is continually dropping and provides an easier alternative to cutting through the particles. An additional source of weakening was provided by the growth of discontinuous precipitate nodules, which have a relatively coarse and therefore a weak structure. Discontinuous precipitation was competitive with general precipitation throughout ageing. Although driven initially by the supersaturation, the nodules were able to continue growing at the expense of the very much finer coherent (or incoherent) general precipitates and attained nearly 7 vol.-% after ageing for 1 week.

The X-ray results will now be discussed. Analysis of the (peak) positions of the " side-bands " in Fig. 2 at the 111, 200, 220, 311, and 222 reflections showed that they could be accounted for reasonably well, after Geisler and Newkirk,[8] by the presence of tetragonal precipitate and matrix phases, both coherent with the original denuded matrix. The unit cell dimensions would be $a_0 = 3{\cdot}6332$ and 3·5374 Å for the tetragonal matrix and precipitate, respectively, both with $c_0 = 3{\cdot}5858$ Å. The diffuseness of the " side-bands " could then be accounted for by postulating a spectrum of tetragonal cells of varying size corresponding to nucleation over a period of time from a matrix of changing composition, but the relative sharpness of the principal reflections could not then be explained.

Alternatively, the tetragonality hypothesis could be discarded and the side-bands attributed to a periodicity of the structure with the diffuseness accounted for by the statistical spread of whatever characteristic dimension was responsible, viz. particle size, particle spacing, or row spacing. Periodic changes in scattering factor could be neglected since copper, nickel, and cobalt atoms have similar scattering factors. Characteristic periodicities, Q_a, of 45, 40, 69, and 126 Å after 1, 5, 15 min, and 5 h ageing at 650° C, respectively, were calculated from the {200} side-band positions applying the usual Daniel and Lipson relation.[19] These will now be compared with the possible characteristic dimensions.

The distribution of row spacings after 5 h ageing, measured parallel to an ⟨001⟩ direction between particle row centres in an (011) foil, peaked at ~ 225 Å. This is nearly a factor of 2 greater than the 126 Å computed above. Furthermore, alignment in rows was not found by electron microscopy at the shorter ageing times, and should in fact have been present after solution-treatment if spinodal nucleation were assumed.

Unfortunately, it did not prove possible to obtain micrographs suitable for measuring average particle dia. for comparison with the Q_a values. However, the typical particle dia. appeared to be ~ half of Q_a after 1–5 min ageing, and similar to Q_a after 5 h ageing. If it were assumed that the volume fraction of precipitate was 0·01 after ageing for 1 min at 650° C the estimated particle spacing for an assumed average particle dia. of 20 Å was a factor of 8 larger than Q_a. If it were further assumed that the volume fraction of precipitate was 0·10 after ageing for 5 h, the estimated spacing for an average particle dia. of 150 Å was in good agreement with Q_a.

Since the particle spacings seem to be too big to account for the observed side-band spacing, the particle dia. appears to be the most plausible source of periodicity. The correct model is then the Guinier random-zone model,[20] modified for 3-dimensional instead of plate-like zones[5] and for the asymmetric alloy case.[7] The possibility that the " side-bands " are simply reflections from tetragonal coherent precipitate and matrix phases seems unlikely since it does not explain the sharpness of the principal reflections. However, it cannot be entirely ruled out; X-ray observations on single crystals should permit a distinction to be made.

From the present data, it appears correct to regard the initial solid solution as decomposing gradually on ageing, so that its lattice parameter moves progressively towards that of the final copper-rich matrix, during which time discrete volumes of three different compositions (and possibly crystal structures) are present with diffuse coherent interfaces, the mismatch being accommodated elastically. The mismatch, particle size, volume fraction of particles, and degree of alignment of particles increase, leading to a 3-dimensional interpenetrating network. Eventually loss of coherency occurs, apparently concurrently with the detection by X-ray diffraction of the two f.c.c. phases now near the equilibrium compositions which they continue to approach. The mismatch is now presumed to be accommodated by dislocation networks; agglomeration and coalescence proceeds, leading to the final structure containing isolated irregular particles.

Acknowledgements

The author would like to thank Mr. J. A. Hugo for general experimental assistance and Mr. L. M. Osika and Mrs. A. M. Davis for the X-ray measurements. He also wishes to record his indebtedness to the late Mr. W. A. Roman for the hardness measurements and light metallography.

References

1. V. A. Phillips, *Trans. Met. Soc. A.I.M.E.*, 1964, **230,** 967.
2. V. A. Phillips, *Acta Met.*, 1966, **14,** 1533.
3. A. J. Ardell, R. B. Nicholson, and J. D. Eshelby, *ibid.*, p. 1295.
4. A. Kelly and R. B. Nicholson, *Progress Materials Sci.*, 1963, **10,** 151.
5. A. Guinier, *Solid State Physics (Advances in Research and Applications)*, 1959, **9,** 293.
6. D. de Fontaine, " Local Atomic Arrangements Studied by X-Ray Diffraction " (edited by J. B. Cohen and J. E. Hilliard), p. 51. **1966:** New York (Gordon and Breach).
7. M. Hillert, M. Cohen, and B. L. Averbach, *Acta Met.*, 1961, **9,** 536.
8. A. H. Geisler and J. B. Newkirk, *Trans. Amer. Inst. Min. Met. Eng.*, 1949, **130,** 101.
9. E. Biedermann and E. Kneller, *Z. Metallkunde*, 1956, **47,** (I), 289: (II), 760.
10. P. J. Tufton Ph.D. Dissertation, Univ. Cambridge, **1963.**
11. R. M. Bozorth, " Ferromagnetism ". **1951:** New York (D. Van Nostrand).
12. W. Guertler and G. Rassmann, *Metallwirtschaft*, 1943, **22,** 1.
13. W. Dannöhl and H. Neumann, *Z. Metallkunde*, 1938, **30,**217.,
14. J. A. Hugo and V. A. Phillips, *Brit. J. Appl. Physics*, 1963, **40** 202.
15. U. Valdrè, *J. Sci. Instruments*, 1962, **39,** 278.
16. V. A. Phillips and J. D. Livingston, *Phil. Mag.*, 1962, **7,** 969.
17. M. F. Ashby and L. M. Brown, *ibid.*, 1963, **8,** 1083.
18. S. L. Sass, T. Mura, and J. B. Cohen, *ibid.*, 1967, **16,** 679.
19. V. Daniel and H. Lipson, *Proc. Roy. Soc.*, 1943, [A], **181,** 368.
20. A. Guinier, *Acta Met.*, 1955, **3,** 510.

Zone Formation in an Austenitic Steel Containing Aluminium and Titanium

F. G. Wilson

The early stages of ageing in a 25% Ni–15% Cr–0·8% Al–4% Ti steel have been studied by resistivity and thin-foil techniques, and the results have been compared with those obtained on an aluminium-free steel. The form of the resistivity changes was found to be similar to that observed in a 4% Ti steel. Below 840° C, the resistivity increased to a maximum which was caused by the formation of coherent spherical zones. At 860° C, the formation of γ' caused a resistivity increase but this was due to the generation of coherency strains at the γ'/austenite interface. Although structurally identical, a clear kinetic difference exists between ordered zones and the γ' precipitate. The addition of aluminium suppressed the formation of cellular Ni_3Ti and reduced the amount of Widmanstätten Ni_3Ti at any temperature, although Fe_2Ti was detected as large grain-boundary particles at the higher ageing temperatures. The spinodal temperature was increased from 730 to 790° C and the zone solvus temperature was increased from 840 to 855° C. Below 730° C, aluminium reduced the rate of growth of the zones and this was attributed to a lower quenched-in vacancy concentration. At 860° C, the nucleation of γ' was reduced by a factor of 30 by the presence of aluminium and this was attributed to the fact that the chemical driving force for the nucleation of f.c.c. Ni_3Ti is greater than for Ni_3 (Al, Ti).

In a recent resistivity and thin-foil electron-microscope investigation[1] the kinetics of the early stages of precipitation in a 25% Ni–15% Cr–4% Ti austenitic steel were studied. If 0·8% Al is added to such a steel, the rapid overageing associated with the formation of cellular Ni_3Ti is considerably retarded.[2,3] However, the effect of aluminium on the kinetics of zone formation in a titanium-bearing austenitic steel is not known, and the present investigation was undertaken to obtain the relevant kinetic data and to compare them with the kinetics of precipitation in an aluminium-free steel.

Experimental Procedure

The steel used had the following composition (wt.-%):

C	Mn	Si	Ni	Cr	Al	Ti	N
0·059	1·13	0·34	25·15	15·39	0·86	4·30	0·01

Manuscript received 20 February 1968. F. G. Wilson, B.Eng., Ph.D., is in the Swinden Research Laboratories, United Steel Co., Rotherham, Yorks.

The method of preparing the wire for the resistivity work was identical to that used for the aluminium-free alloy.[1]

The apparatus used to measure the resistivity was based on one originally designed by Colner and Zmeskal.[4] The mode of operation, which entailed solution-treating for 5 min at 1150° C in vacuum followed by quenching in argon direct to the isothermal ageing temperature, was described in the earlier paper.[1]

The electron-microscope investigation was carried out on separately aged strip material which had been solution-treated at 1150° C and quenched directly into a salt bath.[1]

Experimental Results

Resistivity Changes

The resistivity changes were measured continuously at the ageing temperature and were expressed as a percentage, $\frac{\Delta\rho}{\rho_0} \times 100$, where ρ_0 is the resistivity immediately following the quench and $\Delta\rho = \rho_t - \rho_0$, where ρ_t is the resistivity at time t.

The effect of ageing temperature on the changes in resistivity are shown in Figs. 1–3 and the form of the changes was very similar to that observed in the 4% Ti steel.[1]

To ensure that oxidation was not responsible for the resistivity increases, a number of runs were repeated in dry hydrogen and found to agree with the results obtained in high-purity argon.

Optical Microstructures

Aged wire samples were examined optically to observe any large-scale morphological changes associated with the resistivity changes. Cellular Ni_3Ti precipitate was not observed at any temperature. At temperatures below 800° C a general darkening of the matrix accompanied overageing but resolution of individual precipitates was impossible.

Even after 500 min at 840° C (Fig. 4(*a*)) the predominant precipitate was γ', which was associated with darkening of the matrix. In addition, large angular grain-boundary particles, together with a few isolated particles within the grains, were observed. X-ray diffraction on extracted residues from aged specimens indicated that these particles were h.c.p. Ni_3Ti and Fe_2Ti.

Ageing at 860° C caused considerable growth of the γ' (Fig. 4 (*b*)) and in addition needles of Ni_3Ti were observed together with the large angular grain-boundary particles of Fe_2Ti. After ageing at 900° C, γ' was not observed and growth and coalescence of the Fe_2Ti particles occurred with further precipitation of Ni_3Ti (Fig. 4(*c*)).

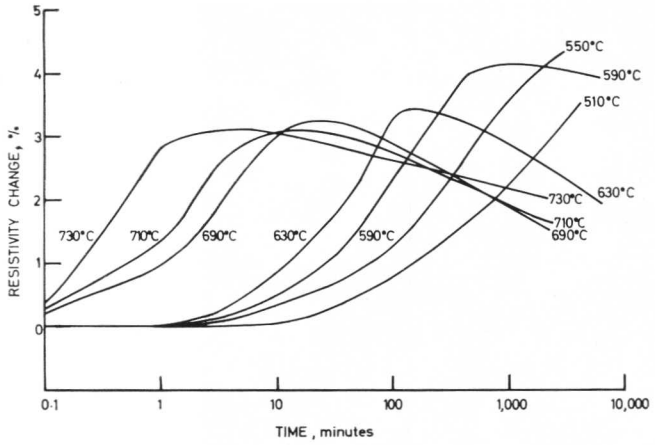

Fig. 1 *Resistivity changes observed on isothermal ageing between* 510 *and* 730° *C.*

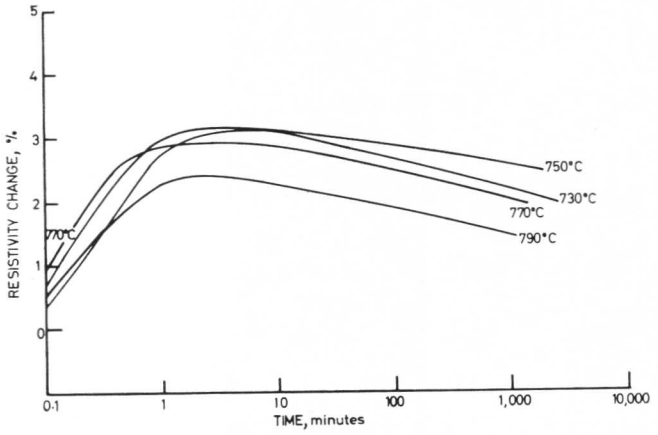

Fig. 2 *Resistivity changes observed on isothermal ageing between* 730 *and* 790° *C.*

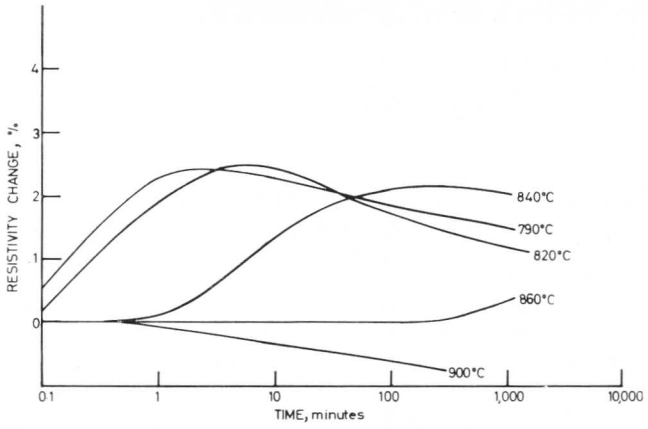

Fig. 3 *Resistivity changes observed on isothermal ageing between* 790 *and* 900° *C.*

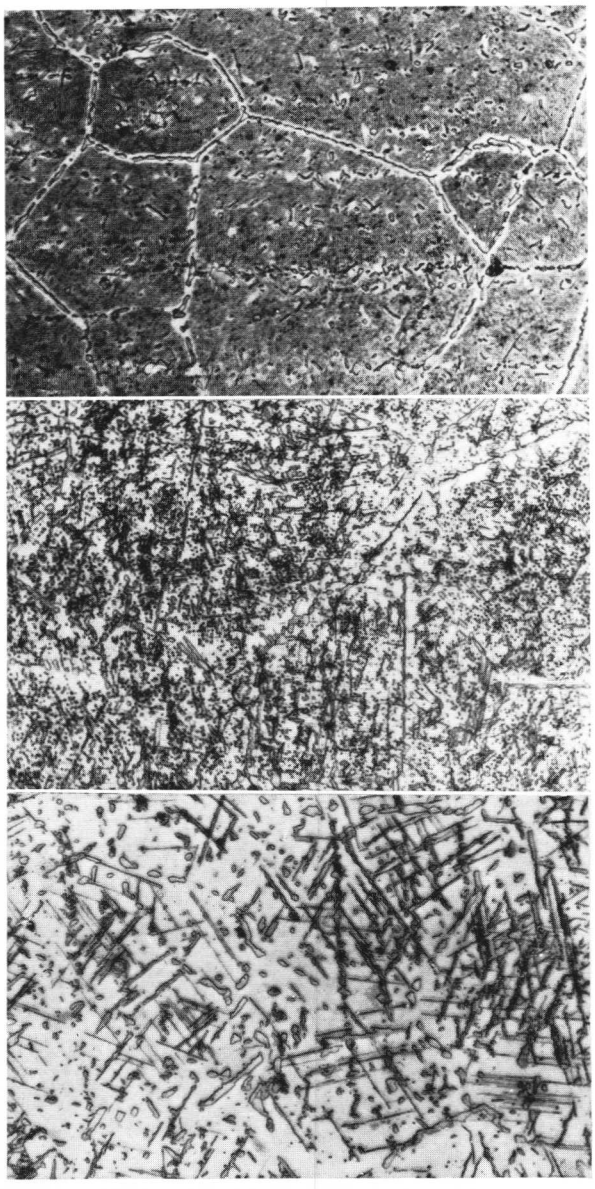

(*a*)

(*b*)

(*c*)

Fig. 4 *Optical microstructures of aged wire specimens.* (a) *Aged* 500 *min at* 840° *C;* (b) *aged* 4100 *min at* 860° *C;* (c) *aged* 5280 *min at* 900° *C.* × 750.

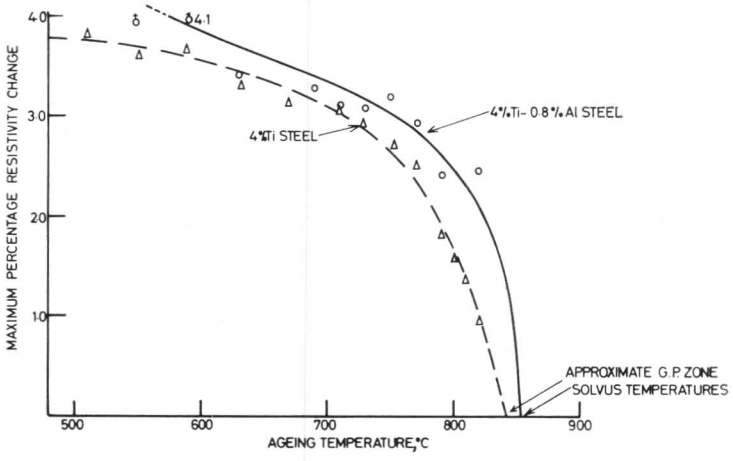

Fig. 5 *Effect of ageing temperature on maximum percentage increase in resistivity.*

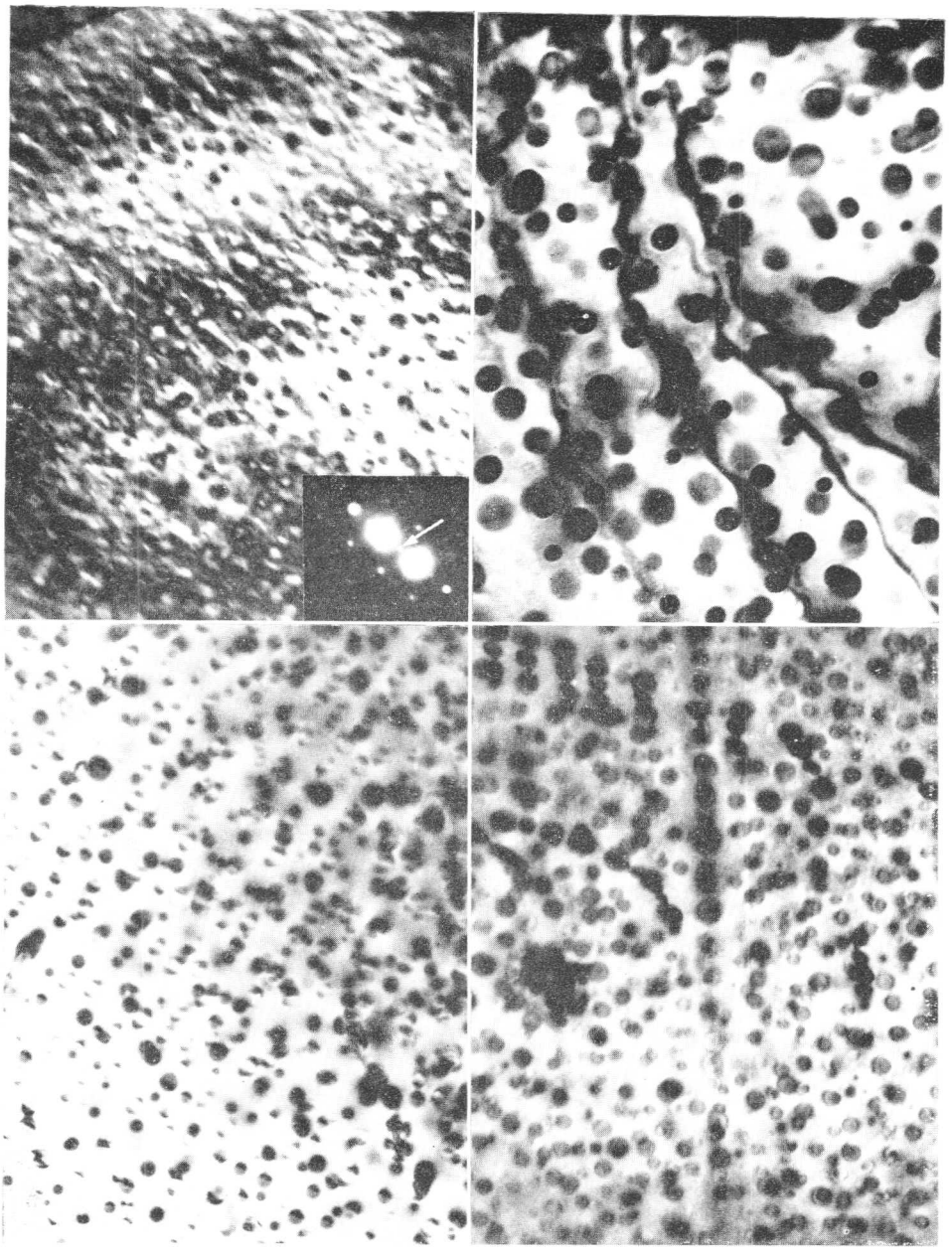

Fig. 6 Effect of ageing temperature on the structure. (a) *Aged* 100 *min at* 840° *C.* × 80,000. (*Note superlattice reflection.*) (b) *Aged* 1000 *min at* 840° *C.* × 80,000. (c) *Aged* 1000 *min at* 860° *C.* × 32,000. (d) *Aged* 1000 *min at* 860° *C.* × 32,000.

Electron Microscopy

In the 4% Ti austenitic steel[1] excellent agreement was found between the morphological and resistivity changes. The general form of the resistivity changes in the present alloy was similar to that observed in the 4% Ti steel and on the basis that the resistivity maximum is due to the presence of zones of critical dia.[5] (~ 10 Å) the extrapolation shown in Fig. 5 indicates that the zone solvus temperature is ~ 855° C. The thin-foil electron-microscope examination confirmed the agreement between the resistivity maximum and the presence of zones, especially below 820° C. However, after 1 min at 840° C the aged steel contained zones although diffraction evidence of ordering was not obtained until after 100 min when γ' particles, ~ 100 Å in dia., were detected (Fig. 6(*a*)). Ageing for 1000 min promoted rapid growth of the γ' (Fig. 6 (*b*)) and, on occasions, trace amounts of cellular Ni_3Ti.

It can be seen that the resistivity and structural changes were not compatible at this temperature, the presence of a fine zone structure after 1 min being associated with a very small resistivity increase. A similar discrepancy was observed in the 4% Ti steel at 820° C.[1]

No evidence for any zone or γ' formation was obtained after 100 min at 860° C, the lack of precipitation confirming the resistivity results. However, ageing for 1000 min at

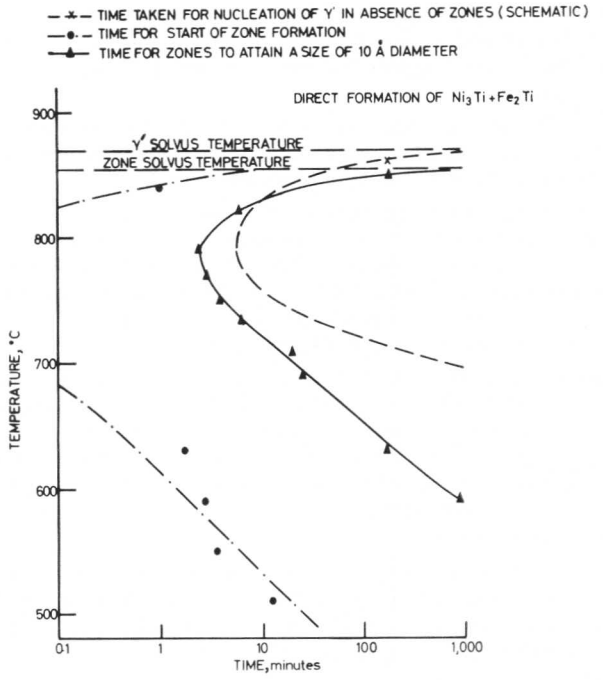

Fig. 7 TTT characteristics for zone, γ', and $Ni_3Ti + Fe_2Ti$ formation.

860° C produced uniformly distributed γ' particles ranging from 600 to 700 Å in diameter (Fig. 6(*c*)).

Widmanstätten Ni_3Ti was also observed and Fig. 6(*d*) illustrates the initiation of an Ni_3Ti platelet by the lining-up of individual γ' particles.

Discussion

The Interpretation of the Changes in Resistivity

The resistivity curves at different ageing temperatures were very similar to those observed in the 4% Ti steel[1] and the thin-foil results showed that the interpretation of the changes was similar. The correlation between the morphological and resistivity changes will therefore be discussed only briefly.

At all Temperatures below 840° C

The resistance increases observed were due to the formation and growth of zones to a critical dia. (~ 10 Å), further growth causing a subsequent decrease. The comparatively rapid decrease in resistivity observed in the 4% Ti steel[1] was due mainly to the formation of cellular Ni_3Ti.

The magnitude of the maximum in the resistivity change is proportional to the number of zones per unit volume and it can be seen from Fig. 5 that the zone density in equilibrium at any temperature decreased with increasing temperature giving a zone solvus temperature of ~ 855° C.

At 860° C

It appears that the increase in resistivity observed at 860° C was due to the coherency strains associated with the growing γ' particles. It was not due to particles attaining a size of ~ 10 Å dia., since the majority of the particles, once nucleated, appeared to grow very rapidly, quickly attaining a size considerably in excess of 10 Å. The possibility that oxidation was contributing to the increase was eliminated when identical results were obtained in dry hydrogen.

On the basis that, depending on ageing temperature, a resistivity increase can be due either to zones attaining a dia.

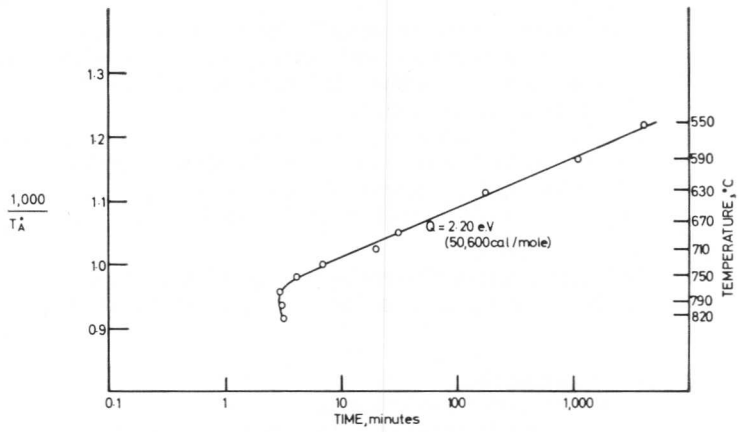

Fig. 8 Reciprocal of the absolute ageing temperature plotted vs. the log time, t_m, to reach the maximum resistivity.

of 10 Å or to the generation of coherency strains at the γ'/austenite interfaces, it must be concluded that at intermediate temperatures, particularly in the range 820–860° C, the observed increases are due to a combination of zone size and coherency strains. At 840° C, for example, the thin-foil and resistivity techniques did not agree, particles of ~ 30 Å being observed after 1 min despite the very small resistivity increase. Although the form of this curve cannot be explained, it is thought that the resistance changes observed were due to both coherency strains and particle size.

The very slow rate of decrease in resistivity observed at 700–800° C was probably due to the growth of large γ' particles, the coherency strains maintaining the resistivity despite the growth of the particles.

At 900° C

A slow but continuous decrease in resistivity was observed at 900° C and was accompanied by coarse heterogeneous precipitation of Ni_3Ti and Fe_2Ti. The decrease observed was typical of systems in which zone or intermediate precipitation does not occur and corresponds to the removal of solute from the matrix.

The Kinetics of Precipitation

Zone Formation

On the basis of the resistivity and thin-foil data, it is possible to present the results in the form of a *TTT* diagram for zone formation[1] (Fig. 7). Between 690 and 820° C, spontaneous zone growth was observed, the maximum rate of growth being observed at 790° C, the spinodal temperature.[1]

The activation energy for the growth of zones below 790° C (corresponding to the migration of solute atoms through the matrix) can be deduced from a plot of the time to attain the maximum resistivity against the reciprocal of the absolute temperature (Fig. 8). Linearity was maintained over the range 550–790° C, the slope giving an activation energy of 50,600 cal/mole. This value was the same as that observed in the 4% Ti steel.[1]

The retardation in the rate of precipitation above 790° C indicated that above this temperature a barrier to nucleation must exist although even at 820° C spontaneous zone growth was observed. At 840° C, an incubation period was observed although metallographically the initial product was indistinguishable from that formed below the spinodal temperature.

γ′ Formation

The G.P.-zone solvus temperature for the present alloy was at ~ 855° C and above this temperature direct nucleation of γ′ occurred after a considerable incubation period. The γ′ solvus temperature occurred at ~ 870° C.

The transformation curve for γ′ formation (Fig. 7) indicates that from 750 to 820° C zone formation preceded the formation of γ′. The effect of this precipitation sequence on the form of the resistivity curves has already been discussed.

Precipitation at 900° C

At 900° C, no zones or γ′ were observed and direct formation of h.c.p. Ni_3Ti[1] and grain-boundary Fe_2Ti occurred after an incubation period.

Sequence of Precipitation

It was demonstrated that in the case of a 4% Ti steel, it is valid to differentiate between a zone and a γ′ precipitate although they are structurally identical.[1] The present work has confirmed that there is a clear kinetic difference between a zone, which forms by migration of solute atoms to produce the required structure, and a γ′ particle which forms after an incubation period by nucleation and growth. A similar kinetic differentiation has been made between zone formation and intermediate precipitate formation in an Al–Mg–Si alloy.[6] The precipitation sequences were temperature-dependent and from 700 to 840° C, the proposed ageing sequence is:

Austenite → Zones → Zones dissolve → Independent nucleation of γ′ probably at dissolving zone/austenite interfaces

Between ~ 850 and 870° C:

Austenite → γ′ → Isolated Ni_3Ti needles.

Between 870° C and the solvus temperature:

$$\text{Austenite} \rightarrow Ni_3Ti + Fe_2Ti$$

The basic precipitation mechanisms are therefore very similar to those occurring in a 4% Ti steel[1] but the addition of 0·8% Al promotes a number of kinetic modifications to the precipitation which will now be discussed in detail.

The Effect of Aluminium on the Precipitation Characteristics of a 4% Ti Steel

The most obvious effect produced by the presence of 0·8% Al on the ageing of a 4% Ti steel is the suppression of the cellular reaction and a reduction in the amount of Widmanstätten Ni_3Ti precipitate.[2,3] However, the presence of aluminium also has a more subtle influence on the precipitation which is not immediately apparent without considering the resistivity and thin-foil data.

The addition of aluminium to a 4% Ti steel in effect increases the solute content and, on this basis alone, such a steel would be expected to exhibit the following characteristics when compared with the aluminium-free steel.

(i) The zone solvus and γ′ solvus temperatures would be increased, together with the true solvus temperature. The effect of alloy content on the solvus temperatures is shown below:

	4·10% Ti Steel	0·8% Al–4·30% Ti
Spinodal temperature	730° C	790° C
G.P.-zone solvus temperature	840° C	855° C
γ′ solvus temperature	870° C	870° C

As expected, therefore, the higher-alloy steel possessed both a higher spinodal and zone solvus temperature than the Ti steel but it would appear that the γ′ solvus temperatures were very similar.

(ii) Below the zone solvus temperature the number of zones in equilibrium at a given temperature would be expected to be higher in the aluminium-bearing steel.

An estimation of the number of zones in equilibrium at a given temperature can be obtained from a measurement of the resistivity peak, which is directly proportional to the density of zones of critical dia. (~ 10 Å). It can be seen from Fig. 5 that the Al–Ti steel did in fact have a higher zone density than the Ti steel at all temperatures.

(iii) The atomic dia. of titanium and aluminium are very similar and, on the basis of a random walk model, the migration rates of these elements would be expected to be very similar. In fact, below the respective spinodal temperatures, the activation energies for solute migration in the Ti and the Al–Ti alloys were identical within experimental error (49,000 and 50,600 cal/mole).

However, below 730° C, the rate of growth of zones to 10 Å dia. was significantly lower in the Al–Ti steel than in the Ti steel; this observation would not be expected solely from a consideration of the respective solute contents.

The addition of trace elements to age-hardening alloys is known to have a marked effect on the rate of zone formation. This is well documented in non-ferrous systems[7] and in the Al–Cu system, for example, the addition of only 0·01% In markedly reduces the zone growth rate.[8] It is suggested that the effect of aluminium in the present alloy is a manifestation of the same phenomenon and is due to a reduction in the concentration of quenched-in vacancies, thereby limiting the transport rate of the solute atoms.

The reason for the decrease in vacancy concentration upon the addition of aluminium is less easy to explain, although it can be discussed in qualitative terms. The atomic dia. for iron, titanium, and aluminium are 2·54, 2·93, and 2·85 Å, respectively.[9] In an austenitic steel containing 4% Ti, much of the distortion associated with the titanium atoms would be minimized by the formation of titanium–vacancy complexes at 1150° C. The reduction in the overall vacancy concentration on the addition of aluminium could be explained as being due to the formation of aluminium–titanium complexes to minimize the solute strain energy. The association of the smaller aluminium atom with a large titanium atom would probably reduce the localized distortion without requiring the formation of a vacancy in the vicinity of the titanium atoms.

At temperatures above the spinodal for the Ti steel (730° C) but below that for the Al–Ti steel (790° C) the rate of zone growth to 10 Å dia. was much faster in the latter steel, thus reversing the trend observed at lower temperatures. However, this effect occurred because above 730° C in the Ti steel, the rate at which zones attained a size of 10 Å dia. was dependent not only on the migration of solute but also on the nucleation of the zones because the chemical driving force for precipitation was much reduced.

At 860° C, the addition of Al to the Ti steel increased the incubation period for the nucleation of γ′ from 10 min to ~ 300 min, i.e. by a factor of 30. In addition the subsequent growth of γ′ was also retarded: after 1000 min the average particle size was ~ 600 Å compared with 800 Å in the Ti steel.[1]

These data show the apparently anomalous effect that above the zone solvus temperature increasing the solute content in the form of added aluminium decreased the nucleation and growth rate of γ'. One possible reason for this is that the addition of Al reduces the quenched-in vacancy concentration owing to the formation of titanium–aluminium complexes. Although this effect is important at low temperatures, particularly below the spinodal, it is unlikely to account for a decrease in nucleation rate by a factor of 30 at 860° C. Alternatively the nucleation barrier for the formation of f.c.c. $Ni_3(Al, Ti)$ may be greater than that for the formation of f.c.c. Ni_3Ti if the chemical driving force for the nucleation of Ni_3Ti is greater than for $Ni_3(Al, Ti)$. Unfortunately no thermodynamic data exist to confirm this point.

Conclusions

A resistivity and thin-foil investigation has been carried out to study the kinetics of precipitation in a 25% Ni, 15% Cr steel containing 4% Ti–0·8% Al and the results have been compared with those previously obtained on a 4% Ti austenitic steel.

At temperatures below ~ 840° C, the growth of zones to a critical dia. (~ 10 Å) causes the resistivity to increase to a maximum. At 860° C the resistivity increase, observed after an incubation period, is due to the formation of coherency strains at the γ'/austenite interface.

The number of zones in equilibrium decreases rapidly with increasing temperature and the zone solvus temperature is ~ 855° C. The maximum rate of zone formation occurs at 790° C, the spinodal temperature, and between this temperature and 840° C the nucleation barrier, although positive, is so low that copious zone formation is still observed.

It has been found that the addition of 0·8% Al to a 25% Ni–15% Cr–4% Ti austenitic steel produces the following effects on the kinetics of precipitation:

(1) The spinodal and zone solvus temperatures are increased by the addition of Al although the γ' solvus temperature appears to be unaltered.

(2) Below the zone solvus temperature, the number of zones in equilibrium at a given temperature is higher in the Al–Ti steel.

(3) Below the spinodal temperature of the Ti steel (730° C) the rate of growth of zones to 10 Å dia. is considerably faster than that observed in the Al–Ti steel.

(4) Below 730° C, the activation energies for solute migration in the two alloys are identical and the difference in zone growth rate can be attributed to a lower quenched-in vacancy concentration in the Al–Ti steel.

(5) At temperatures above the spinodal for the Ti steel (730° C) but below that for the Al–Ti steel (790° C) the rate of zone growth to 10 Å dia. is faster in the latter steel, thus reversing the trend observed at lower temperatures. This is due to the presence of a nucleation barrier above 730° C in the Ti steel.

(6) At 860° C the nucleation rate of γ' is reduced by a factor of 30 by the addition of 0·8% Al; the growth rate is also reduced. These effects are attributed to the lower quenched-in vacancy concentration in the presence of Al, and also to the greater chemical driving force for the nucleation of f.c.c. Ni_3Ti compared with $Ni_3(Al, Ti)$.

(7) At 900° C the direct formation of Ni_3Ti (h.c.p.) is much reduced in the presence of 0·8% Al and large angular grain-boundary plates of Fe_2Ti are formed.

Acknowledgements

The author wishes to thank Dr. F. H. Saniter, O.B.E., Director of Research, United Steel Companies, Ltd., for permission to publish the paper and Mr. F. B. Pickering for helpful discussions during the progress of the work.

References

1. F. G. Wilson and F. B. Pickering, *Acta Met.*, 1968, **16,** 115.
2. B. R. Clark and F. B. Pickering, *J. Iron Steel Inst.*, 1967, **205,** 70.
3. F. G. Wilson and F. B. Pickering, *ibid.*, 1966, **204,** 628.
4. W. H. Colner and O. Zmeskal, *Trans. Amer. Soc. Metals*, 1952, **44,** 1, 158.
5. N. F. Mott, *J. Inst. Metals*, 1937, **60,** 267.
6. D. W. Pashley, M. H. Jacobs, and J. T. Vietz, *Phil. Mag.*, 1967, **16,** 51.
7. A. Kelly and R. B. Nicholson, *Progress Materials Sci.*, 1963, **10,** (3), 151.
8. K. M. Entwistle and A. J. Perry, *J. Inst. Metals*, 1966, **94,** 24.
9. W. Hume-Rothery and G. V. Raynor, " The Structure of Metals and Alloys ". **1962:** London (Inst. Metals).

The Decomposition of Concentrated Al–Zn Alloys

A. J. Ardell, K. Nuttall, and R. B. Nicholson

The decomposition of a series of Al–Zn alloys has been investigated by electron microscopy. Three of the alloys fall within the miscibility gap of the Al–Zn system and show a "modulated" structure on ageing which is found to be not necessarily associated with spinodal decomposition. The fourth alloy decomposes by a eutectoid reaction to give a lamellar structure but when rapidly quenched it gives a very fine mixture of the two phases which is interpreted in terms of spinodal decomposition.

The decomposition of supersaturated Al–Zn alloys has been studied extensively by many techniques.[1] Recent electron-metallographic and X-ray studies[2,3] suggest that the dilute (up to 15 at.-% Zn) f.c.c. aluminium-rich alloys decompose to give the aluminium-rich solid solution and the following series of precipitates:

Spherical G.P. zones → rhombohedral α' → cubic α' → zinc.

The rhombohedral α' phase differs only slightly in lattice parameter from the cubic α' phase.

The more concentrated Al–Zn alloys have been investigated less thoroughly. Graf and Lenormand[4] showed that an aged 22 at.-% Zn alloy exhibited X-ray "side-bands", which are often associated with spinodal decomposition.[5] Rundman and Hilliard[6] have recently used X-ray small-angle scattering to obtain convincing evidence that the same alloy does in fact decompose spinodally at room temperature. There has since been some discussion[7,8] of the interpretation of their results.

The most recent phase diagram for the Al–Zn system[9,10] shows the existence of a second high-temperature f.c.c. phase, γ, which exists over an approximate composition range of 49–63 at.-% Zn and decomposes at 276°C by a eutectoid reaction. This reaction has been studied by Garwood and Hopkins,[11] who showed that more than one type of decomposition product occurred depending on the transformation temperature.

Experimental

The alloys used in the present investigation were made from high-purity materials and contained 28·4, 39·3, 50·3 at.-% Zn (corresponding, respectively, to the aluminium-rich side, the critical point, and the zinc-rich side of the miscibility gap) and 59·0 at.-% Zn, which is the eutectoid composition. Extensive segregation was present in the cast blocks but portions of the ingot were selected to give strip material (after hot rolling) that differed by $< \pm 0{\cdot}25$ at.-% Zn in composition, from sample to sample. The three low-zinc alloys were solution-treated for ½ h at 400°C and the eutectoid alloy for 3 h at 380°C. Because of the known tendency for Al–Zn alloys to decompose during quenching to room temperature,[12,13] the specimens were quenched from the solution-treatment temperature directly into the ageing bath (salt or oil). After ageing they were quenched and stored at −10°C to prevent further decomposition at room temperature.

Thin foils were prepared by the disc method for the three low-zinc alloys, using a final electropolishing solution of 30% nitric acid and 70% methyl alcohol at −40°C. Foils from the eutectoid alloy were prepared using the window method and an electropolishing solution of 15% perchloric acid in methyl alcohol at −50°C. Foils from partly decomposed alloys had a tendency to decompose further under observation in the electron microscope and this produced a number of spurious effects on electron-diffraction patterns.

Results

The 28·4, 39·3, and 50·3 at.-% Zn Alloys

The characteristics of the decomposition products of the three low-zinc alloys were identified by quenching foils to 280°C and ageing for times of 7 sec to 1 min at that temperature. Fig. 1 is an example of the microstructure found in all three alloys. The structure has a "modulated" appearance and seems to consist of plate-shaped precipitates. The morphology of the individual plates can be seen more clearly in Fig. 2. The diffraction pattern from this area shows 111 reflections which are split. In general these characteristics are similar to those for the α' plates in the more dilute alloys, i.e. plates on {111} matrix planes which cause satellite reflections by virtue of their departure from cubic symmetry.[1,3] The modulated appearance is, however, more marked than in the dilute alloys.

The modulated structure is evidently fully developed after 7 sec (which was the shortest ageing time we could use) and only coarsens with further ageing. The rapidity of decomposition and the observation of a modulated structure suggest that the mode of precipitation is spinodal decomposition. The main difference between this and other spinodal structures in metallic systems[14] is that the modulations lie parallel to {111} matrix planes rather than {100}.

The next series of experiments was designed to establish whether there was any sharp change in the morphology of the decomposition product as the specimens were aged for fixed times (30 sec) at successively higher ageing temperatures. Typical micrographs of the 28·4% alloy are shown in Fig. 3. Extensive homogeneous precipitation in a modulated form is observed for an ageing temperature of 310°C; at 315°C fewer precipitates are present, but these are still apparently homoge-

Manuscript received 3 July 1968. A. J. Ardell, B.S., M.S., Ph.D., is in the W. M. Keck Laboratory of Engineering Materials, California Institute of Technology, U.S.A. Professor R. B. Nicholson, M.A., Ph.D., A.I.M., and K. Nuttall, B.Sc. M.Sc., are in the Department of Metallurgy, Faculty of Science, University of Manchester.

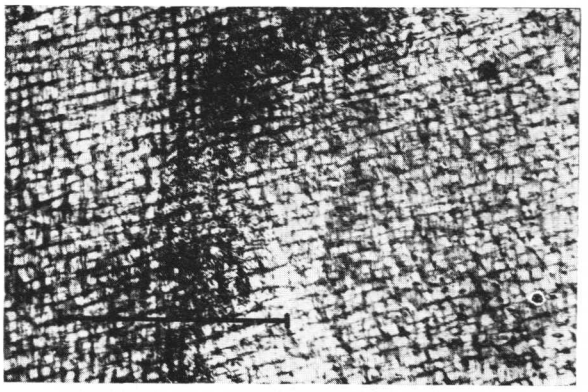

Fig. 1 Micrograph of the 39·3% Zn alloy aged 30 sec at 280°C, showing the "modulated" appearance of the α/α' structure.

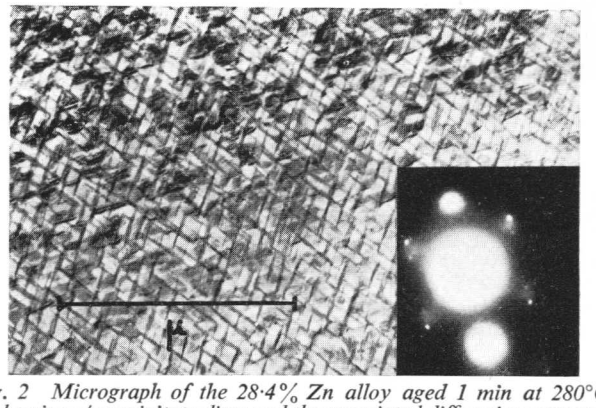

Fig. 2 Micrograph of the 28·4% Zn alloy aged 1 min at 280°C, showing α' precipitate discs and the associated diffraction pattern.

neously nucleated; at 320°C only heterogeneous precipitation on dislocations is apparent. Clearly the range 310–320°C is critical for this alloy. Similar results were found for the other two alloys, the critical ranges being 335–340°C for the 39·3% alloy and 310–320°C for the 50·3% alloy. These temperatures are well within the $\alpha+\alpha'$ miscibility gap and could represent either points on the *coherent* phase boundary for $\alpha+\alpha'$, the chemical spinodal, or the coherent spinodal (see Cahn[15] for a discussion of these concepts).

To distinguish between these possible interpretations of the "critical" temperature, experiments were carried out on the 28·4% alloy. Samples were aged for 2 min at 280°C, quenched to 0°C, and then aged at 320°C. If the critical temperature lies on the coherent spinodal, precipitation in the specimen directly quenched to 320°C (Fig. 3(*c*)) may have been prevented by the presence of a nucleation barrier to precipitation at this temperature. In that case the precipitate formed at 280°C should undergo rapid growth on re-ageing at 320°C. On the other hand, if the critical temperature represents the coherent phase boundary, the precipitate formed at 280°C will dissolve on re-ageing at 320°C. The results of the experiment are shown in Fig. 4, where it is apparent that the precipitate has almost completely dissolved after 1 min at 320°C. This suggests that the second hypothesis is correct.

If a specimen is aged for a long time at 320°C, either after direct quenching or after first ageing for 2 min at 280°C, large semi-coherent α' particles are formed (Fig. 4(*d*)), which confirms the interpretation of the re-ageing experiment. It is clear that there is a substantial nucleation barrier to the formation of the semi-coherent α' phase at 320°C and that

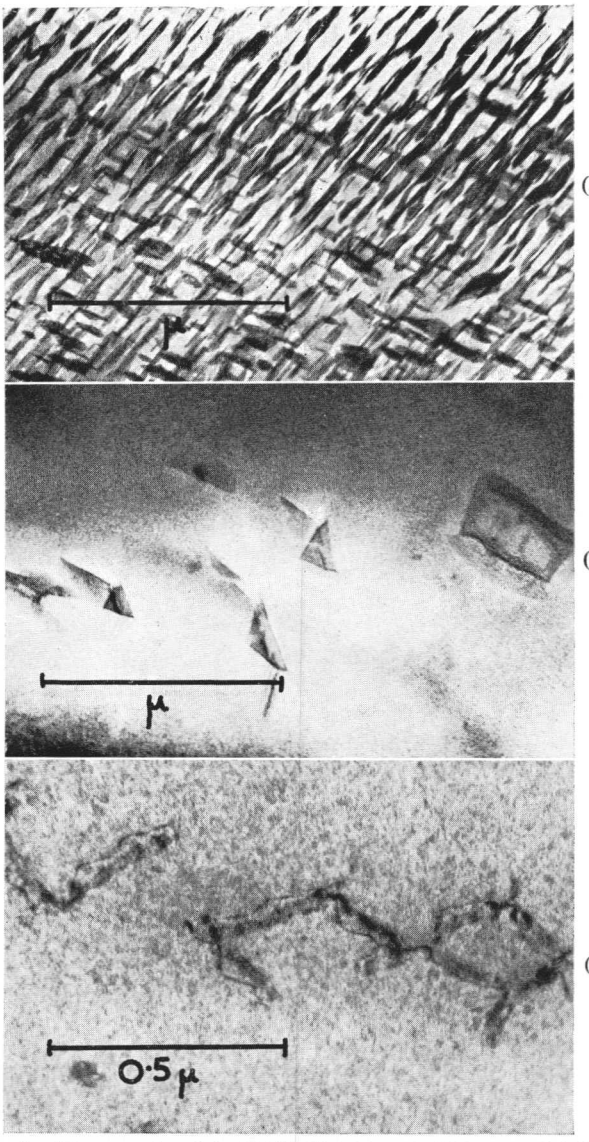

Fig. 3 Micrographs of the 28·4% Zn alloy aged 30 sec at (a) *310,* (b) *315, and* (c) *320°C, illustrating the existence of a "critical temperature" at ~ 315°C. The precipitates in* (c) *have nucleated heterogeneously on dislocations in the matrix.*

coherent α' particles formed at 280°C are not able to act as nuclei for the semi-coherent phase on re-ageing at 320°C.

Further experiments on the 39·3% and 50·3% alloys led to the same conclusion; the critical temperatures represent the coherent α/α' solvus.

The 59·0 at.-% Zn Eutectoid Alloy

The normal decomposition mode of this alloy produced a lamellar structure, as seen in Fig. 5. The two phases are the aluminium-rich and the zinc-rich solid solutions and the structure is entirely typical of other eutectoid decompositions. As the decomposition temperature was reduced the spacing of the lamellae decreased, as expected (cf. Figs. 5(*a*) and (*b*)). However, at sufficiently low decomposition temperatures, e.g. below room temperature, the structure of the decomposition product changed completely. The process became continuous rather than cellular and the two phases were precipitated in approximately equiaxed form (Fig. 6). This structure coarsen-

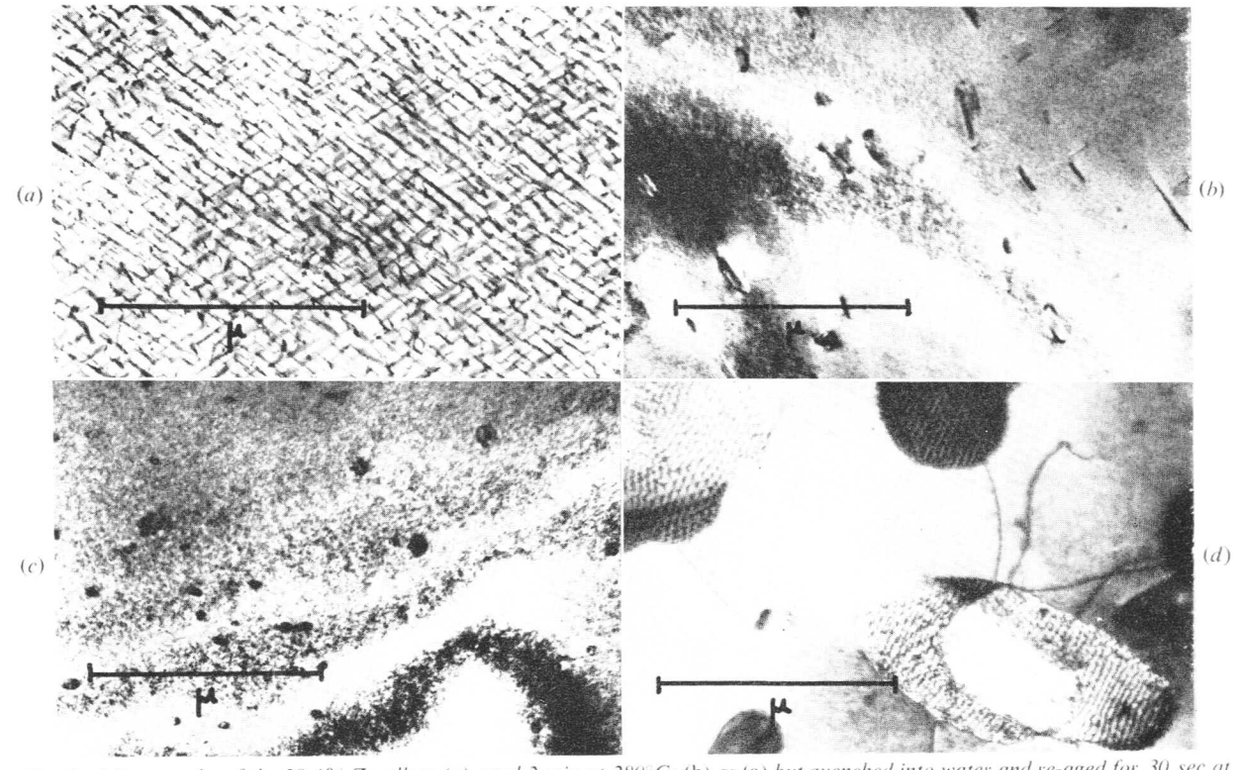

Fig. 4 Micrographs of the 28·4% Zn alloy: (a) *aged 2 min at 280° C;* (b) *as* (a) *but quenched into water and re-aged for 30 sec at 320° C;* (c) *as* (b) *but re-aged for 1 min;* (d) *as* (b) *but re-aged for 2 h; showing dissolution of coherent α′ precipitates and subsequent growth of semi-coherent α′ precipitates.*

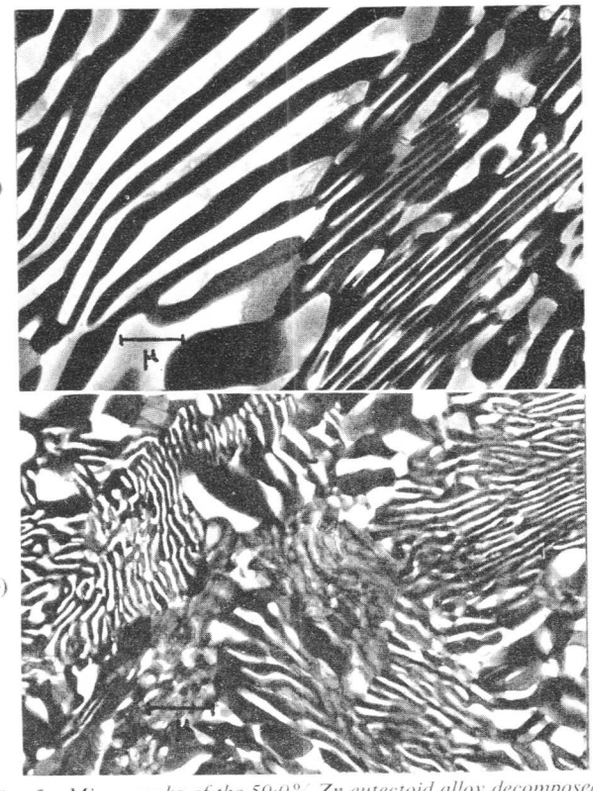

Fig. 5 Micrographs of the 59·0% Zn eutectoid alloy decomposed at (a) *250 and* (b) *150° C, showing decrease in interlamellar spacing with increasing undercooling.*

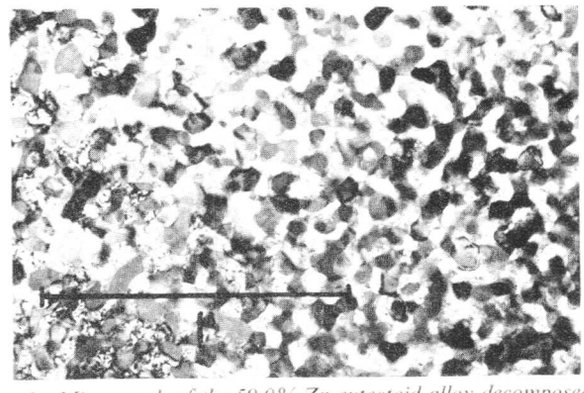

Fig. 6 Micrograph of the 59·0% Zn eutectoid alloy decomposed at −45° C, showing a two-phase equiaxed structure.

ed rapidly even at room temperature, though occasionally foils were obtained that showed microstructures thought to represent the earliest stages of the decomposition process (Fig. 7(*a*)). These bear a remarkable resemblance to micrographs published by Cahn and Charles[16] showing spinodal decomposition in glass (cf. Figs. 7(*a*) and (*b*)). The change in microstructure observed as the decomposition temperature is decreased is consistent with the hypothesis of Garwood and Hopkins,[11] who proposed a change in the mode of decomposition at ~100° C on the basis of kinetic measurements. The current experiments suggest that the critical temperature for the change in a 59·0 at.% alloy is near room temperature.

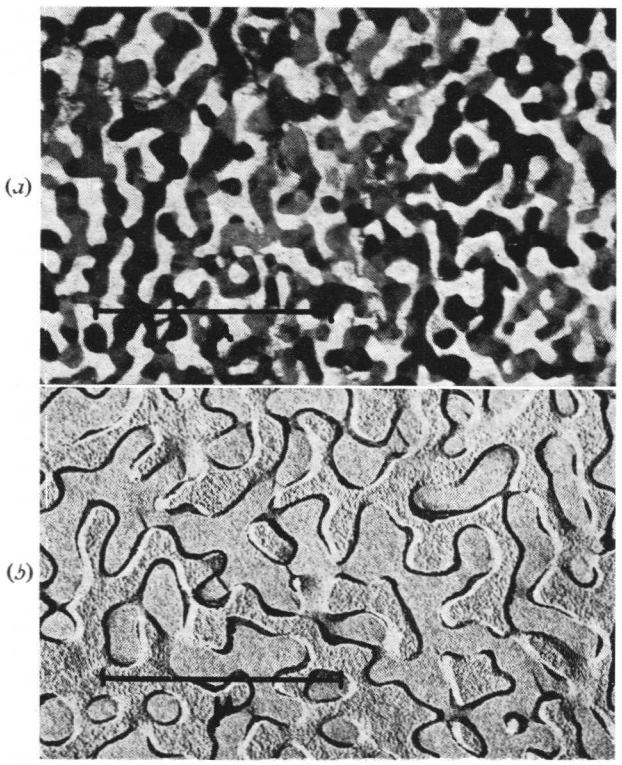

Fig. 7 A comparison of (a) *an earlier stage in the decomposition of the specimen in Fig. 6 and* (b) *a micrograph of spinodal decomposition in a glass.*[16]

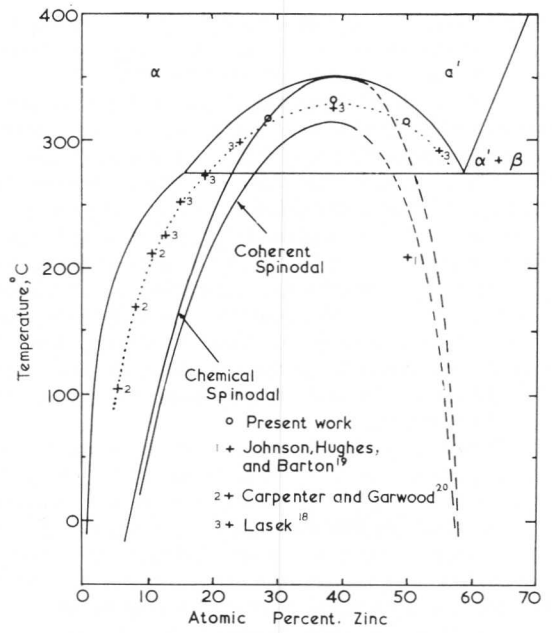

Fig. 8 Part of the phase diagram of the Al–Zn system published in Ref. (6), *showing calculated spinodal curves*[6] *and the experimental values for the coherent solubility curve obtained from the present work compared with "reversion" temperatures measured by other workers.*[18,19,20] *The dotted line is the proposed α/α' coherent solvus.*

Discussion

There have been a number of attempts to relate the form of the miscibility gap in the Al–Zn system to the metastable phase boundaries for G.P. zones and for α'.[1,3,17–21] The possibility of spinodal decomposition has been implicit in the discussion in several of these papers. We will now discuss these results in the light of the present observations.

Let us deal first with the non-eutectoid alloys. Comparing our results with those of Carpenter and Garwood,[3] it is clear that we are concerned with the decomposition of the high-temperature α phase into the aluminium-rich f.c.c. α solid solution and the zinc-rich coherent rhombohedral α' phase, except for long ageing times at high temperatures, Fig. 4(*d*), where the latter phase is in its semi-coherent cubic form. The experiments clearly show the existence of "critical temperatures" in the nucleation behaviour of the decomposition products, and the re-ageing experiment (Fig. 3) indicates that these temperatures are to be identified with the coherent α/α' phase boundary rather than with the coherent spinodal. The measured critical temperatures for the three alloys are plotted in Fig. 8 which is taken in part from the paper by Rundman and Hilliard[6] and contains the chemical and coherent spinodal curves calculated by these authors. (It should be pointed out that the chemical spinodal curve has little meaning, since the early stages of spinodal decomposition necessarily involve the production of coherent phases whereas the chemical spinodal refers to non-coherent phases. Both spinodal curves are shown in Fig. 8 to illustrate the temperature depression of the coherent spinodal with respect to the chemical spinodal caused by taking into account the elastic energy of the coherent phases[15]).

At present it is not clear whether the rhombohedral form of the α' phase should be regarded as a second transition phase or merely as the coherent form of the cubic α' transition phase with the slight distortions of the lattice parameter caused by coherency strains. We shall assume that the latter is true, which means that the critical temperatures measured correspond to the coherent phase boundary (as defined by Cahn[15]) for the α/α' phase equilibrium. As such, the measurements are in excellent agreement with "reversion" temperatures determined for a variety of alloys by Carpenter and Garwood[20] and by Lasek[18] (Fig. 8), though in both cases these authors interpreted their results in terms of the metastable solvus for G.P. zones rather than for α'. However, it is possible that there is only a small temperature difference between these two and, furthermore, the present results suggest that the heat-treatments used by Lasek[18] would give a structure consisting of rhombohedral α' rather than G.P. zones. The coherent α/α' phase boundary is also well positioned with respect to the coherent spinodal calculated from thermodynamic data by Rundman and Hilliard.[6] The critical points, which in theory should coincide, differ by only $\sim$ 10 degC, and this is further evidence for the correctness of our interpretation. However, it should be pointed out that substantially lower "reversion" temperatures have been reported by Borelius[21] and Johnson, Hughes, and Barton,[19] and their results cannot be fitted to our curve in Fig. 8. These authors used indirect experimental techniques, unsupported by metallographic evidence, and it is possible that they measured the G.P. zones $\rightarrow \alpha'$ transition (i.e. simply a less stable phase transforming to a more stable phase) which usually occurs in the range 100–200° C on heating, rather than the true reversion of the structure to a solid solution.

The question remains as to whether there is any evidence of spinodal decomposition in the non-eutectoid alloys. There is no detectable change in the microstructure, (Fig. 3), near the calculated coherent spinodal temperature and we have already seen that the apparent "modulated" structure is not

necessarily related to decomposition by a spinodal mode. (In this case, as in Ni–Al,[22] it may result from selective coarsening of initially randomly distributed particles.) There is no further change in microstructure as the decomposition temperature is lowered until spherical G.P. zones replace the rhombohedral α' platelets as the first-formed precipitate in the range 0–150°C. It is conceivable that this change represents the onset of spinodal decomposition in non-eutectoid alloys and that it occurs at lower temperatures than expected from the calculated curve in Fig. 8 for reasons of ease of formation of the α' phase by conventional nucleation, as envisaged by Cahn.[23] However, it is also possible that G.P. zones merely represent a conventionally nucleated transition phase. This uncertainty in interpretation already exists in other systems forming G.P. zones[24] and the present paper throws no further light on the problem.

We will now consider the results on the eutectoid alloy. The decomposition mode at temperatures in the range 100–270°C is typical of other eutectoid systems and requires no further discussion. At low decomposition temperatures, other eutectoid systems normally show bainitic or martensitic structures, but no such change occurs in the present case. Instead, there is a complete change to a continuous mode of precipitation (Fig. 7(*a*)) which consists, in the earliest stages, of a mixture of two f.c.c. phases, one zinc-rich and the other aluminium-rich. The obvious interpretation is that normal eutectoid-type decompositions have been suppressed by prior spinodal decomposition of the high-temperature phase. The remarkable similarity between this structure and the structure observed in decomposed glasses (cf. Figs. 7(*a*) and (*b*)) supports the view that the present results represent the first uncontroversial case of metallographic evidence for spinodal decomposition in metallic systems. The later stages of the decomposition process consist of the nucleation of h.c.p. zinc grains from the zinc-rich component of the spinodal structure, followed by grain growth to give a fine equiaxed mixture of the zinc and aluminium terminal solid solutions, (Fig. 6).

If it is accepted that Fig. 7(*a*) represents spinodal decomposition, it is necessary to explain why the microstructure is similar to that of an isotropic non-crystalline material such as glass, rather than to the "modulated" structure interpreted as spinodal decomposition in other metallic systems.[14] It is likely that elastic anisotropy is the governing factor. Aluminium is one of the more isotropic metals ($2c_{44}/(c_{11}-c_{12}) = 1{\cdot}24$) and the addition of zinc to give the f.c.c. α solid solution is thought to make the anisotropy factor more nearly unity.[3,25] Thus, it is quite possible that the other high-temperature phase, the f.c.c. γ, is almost perfectly isotropic, resulting in decomposition in all directions in the crystal being equally favoured[26] rather than a preference for ⟨100⟩ directions as shown by most anisotropic materials.

Conclusions

(1) The rapid decomposition of concentrated, non-eutectoid alloys leads to the formation of a "modulated" structure as a result of cooling below the coherent α/α' phase boundary, and not necessarily as a result of spinodal decomposition.

(2) A eutectoid Al–Zn alloy shows a clear transition from a lamellar mode of decomposition to a spinodal structure at about room temperature. The structure produced by spinodal decomposition is typical of a parent lattice that is elastically isotropic.

References

1. A. Kelly and R. B. Nicholson, *Progress Materials Sci.*, 1963, **10**, 149.
2. M. Simerska and V. Synecek, *Acta Met.*, 1967, **15**, 223.
3. G. J. C. Carpenter and R. D. Garwood, *Metal Sci. J.*, 1967, **1**, 202.
4. R. Graf and M. Lenormand, *Compt. Rend.*, 1964, **259**, 3494.
5. M. Hillert, M. Cohen, and B. L. Averbach, *Acta Met.*, 1961, **9**, 536.
6. K. B. Rundman and J. E. Hilliard, *ibid.*, 1967, **15**, 1025.
7. V. Gerold and W. Merz, *Scripta Met.*, 1967, **1**, 33.
8. J. E. Hilliard and K. B. Rundman, *ibid.*, p. 37.
9. A. A. Presnyakov, Yu. A. Gorban', and V. V. Chervyakova, *Zhur. Fiz. Khim.*, 1961, **35**, 1289.
10. G. R. Goldak and J. G. Parr, *J. Inst. Metals*, 1963–64, **92**, 230.
11. R. D. Garwood and A. D. Hopkins, *ibid.*, 1952–53, **81**, 407.
12. C. Panseri and T. Federighi, *Acta Met.*, 1960, **8**, 217.
13. E. L. Huston, J. W. Cahn, and J. E. Hilliard, *ibid.*, 1966, **14**, 1053.
14. R. B. Nicholson and P. J. Tufton, *Z. angew. Physik*, 1966, **21**, 59.
15. J. W. Cahn, *Acta Met.*, 1962, **10**, 907.
16. J. W. Cahn and R. J. Charles, *J. Phys. Chem. Glasses*, 1965, **6**, 181.
17. V. Gerold and W. Schweitzer, *Z. Metallkunde*, 1961, **52**, 76.
18. J. Lasek, *J. Inst. Metals*, 1967, **95**, 320.
19. A. A. Johnson, E. J. Hughes, and P. W. Barton, *ibid.*, 1966, **94**, 186.
20. G. J. C. Carpenter and R. D. Garwood, *ibid.*, 1966, **94**, 301.
21. G. Borelius, *J. Metals*, 1951, **3**, 477.
22. A. J. Ardell and R. B. Nicholson, *Acta Met.*, 1966, **14**, 1295.
23. J. W. Cahn, *ibid.*, 1961, **9**, 795.
24. G. W. Lorimer and R. B. Nicholson, this vol., p. 36.
25. R. S. Leigh, *Phil. Mag.*, 1951, **42**, 876.
26. J. W. Cahn, *Acta Met.*, 1962, **10**, 179.

Precipitation Phenomena in Gold–Platinum Alloys

G. Kralik, J. Weise, and V. Gerold

The early stages of precipitation in gold–platinum alloys have been examined by resistivity measurements on alloys containing 15–25 and 55–65 wt.-% gold. The resistivity measurements were performed on polycrystalline wire specimens of 0·4 mm dia. The aim of the experiments was to establish the existence of a coherent miscibility gap inside the stable incoherent gap. Furthermore, the kinetics of spinodal decomposition was measured at the very beginning, for comparison with the theory advanced by Cahn.[1]

Evidence for the existence of a coherent miscibility gap inside the incoherent gap has been obtained by electrical-resistivity measurements during reheating the samples after appropriate ageing at lower temperatures. The experiments were performed in a gradient furnace, where the temperature changes were produced by moving the specimen in the furnace. The resistivity were measured as a voltage difference against a reference specimen of pure platinum at the same temperature, keeping the electric current in both specimens constant. As an example, Fig. 1 shows the results for a specimen pre-annealed at 770° C for various times. For very short annealing periods the reheating curves merge into the curve for the solid solution far below the temperature of the stable miscibility gap, at a temperature T_c. With increasing annealing time the step at T_c is still observed, but the curve will no longer reach the line for the solid solution at this temperature. This occurs in a second step at the temperature T_i of the stable-gap limit. This result is interpreted as follows. In the alloy two different types of precipitate are present. The coherent type is developed during the beginning of ageing. It dissolves at the temperature T_c. With increasing annealing time, the coherent precipitate is converted into the incoherent type which dissolves at the temperature T_i. The experimental results are given in Fig. 2, where the vertical lines indicate the range of redissolution of the coherent precipitates. It is believed that the limit of the gap is near the lower ends of these marks.

To determine the beginning of the decomposition process, a second set of experiments was undertaken where the specimens were heated to the homogenization temperature by direct current and then quenched into the annealing salt bath in the range 450–900° C. Again, the resistivity change $\dot{\rho}$ was measured using oscilloscope and recorder methods. The influence of the quenched-in vacancies could be clearly observed in the kinetics, especially at lower ageing temperatures. It is shown most clearly in a plot of log $\dot{\rho}$ vs. the resistivity ρ instead of time t. A change of slope in the curve marks the instant when most of the quenched-in vacancies have annealed out.

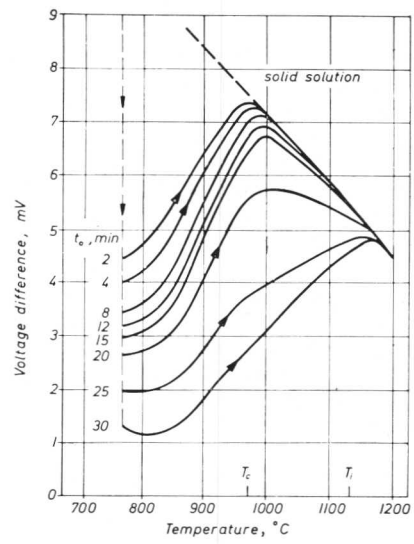

Fig. 1 Reheating curves for a Pt–20% Au alloy pre-annealed at 770° C for various times.

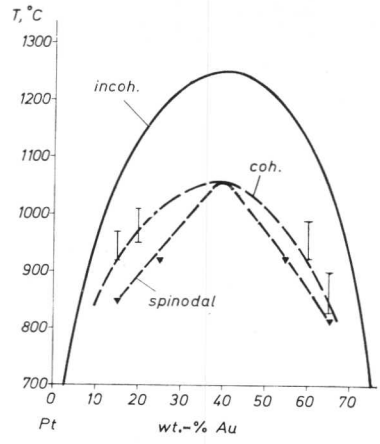

Fig. 2 Coherent and incoherent miscibility gaps in the platinum–gold system.

From an Arrhenius plot of the corresponding time, an activation energy is found which is interpreted as being approximately the activation energy E_m of vacancy diffusion. The results are listed in Table I. E_m varies from 1·12 to 1·29 eV.

Manuscript received 3 July 1968. Professor V. Gerold, Dr.rer.nat., G. Kralik, Dr.phil., and J. Weise, Dipl.Phys., are at the Institut für Metallkunde, Max-Planck-Institut für Metallforschung, Stuttgart, Germany.

TABLE I

Values of E_m, Q, and T_s Obtained Experimentally

% Au	E_m, eV	Q, eV	T_s, °C
15	—	—	850
25	1·29	2·38	900
55	1·12	1·60	920
65	1·25	1·45	820

To obtain the resistivity change at $t = 0$ without the influence of the quenched-in vacancies an extrapolation method was used in the log $\dot{\rho}$ vs. ρ plots. Fig. 3 shows the result, where $\dot{\rho}$ $(t = 0)$ is plotted against the ageing temperature for the four alloys investigated. The broken curves represent the uncorrected values of $\dot{\rho}$ $(t = 0)$ including the influence of the quenched-in vacancies.

According to the theory of spinodal decomposition,[1] concentration fluctuations with an amplitude A and a wavenumber β can be defined. For each temperature T below the spinodal temperature T_s, a characteristic wave number $\beta_m(T)$ exists, for which the growth rate A of the fluctuation at time $t = 0$ is a maximum. Using the regular-solution approximation and assuming that $\dot{\rho} \sim \beta_{mA}$ (β_m), it follows approximately that

$$\dot{\rho}\,(t = 0) \simeq (T_s - T)^{5/2} \exp(-Q/RT) \quad \ldots (1)$$

The full lines in Fig. 3 are curves fitted to the experimental points according to equation (1). From this best-fit approximation the parameters Q and T_s can be obtained. These are listed in Table I.

The values of Q are widely scattered. They are much too small for the alloys containing 65 and 55% Au when compared with the results of other authors.[2–4] Only the value for the 25% alloy is reasonable. In the case of the 15% alloy, no analysis was possible. Here the highest values of $\dot{\rho}$ were observed.

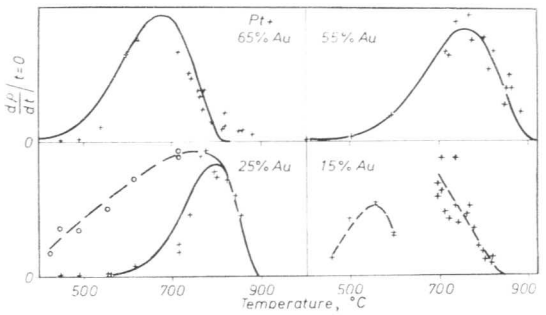

Fig. 3 Rate of resistivity change at $t = 0$ *as a function of annealing temperature.* ○ = *uncorrected measurements (given only for the 55% Au alloy).* + = *corrected measurements. Solid curves are based on equation* (1).

The only reliable result of this analysis seems to be the spinodal temperature, T_s. In Fig. 2 these temperatures are marked as triangles. According to our result the spinodal appears to lie asymmetrically with reference to the coherent miscibility gap, which is not in agreement with theoretical estimates.[5] According to these estimates the horizontal distance between the spinodal and the coherent solvus should be ~ 1/5 of the total width of the solvus. This is not observed on the gold-rich side of this system.

Since the resistivity measurements do not yield a decisive proof for or against the model of spinodal decomposition, X-ray measurements of the side bands were undertaken on flat foils of 0·4 mm thickness. The analysis is still under way but, since only the later stages of the decomposition can be analysed quantitatively, it appears to be difficult to derive proof of the validity of the spinodal decomposition model from these experiments.

References

1. J. W. Cahn, *Acta Met.*, 1961, **9**, 795.
2. R. W. Carpenter, *ibid.*, 1967, **15**, 1567.
3. A. Bolk, *ibid.*, 1958, **6**, 59.
4. J. Mortlock, *Phil. Mag.*, 1960, **5**, 803.
5. H. E. Cook and J. E. Hilliard, *Trans. Met. Soc. A.I.M.E.*, 1965, **233**, 142.

Discussion

Professor V. GEROLD (Max Planck Institute, Stuttgart, Germany): I should like to ask whether anyone has tried to calculate the absolute scattered intensity. I fear that because some decomposition has occurred during the quench, there is a big intensity contribution from concentration fluctuations that are relatively large. We found, especially when comparing the experiments of Rundman and Hilliard* for Al–Zn, that this intensity is so great that there must already be an average concentration fluctuation of the order of 30% present after quenching.† Such a high fluctuation is already consistent with a two-phase model where the second phase has reached its equilibrium concentration. I fear that similar arguments can be advanced about the paper of Tomozawa *et al.* The question is whether the theory of spinodal decomposition is valid at this stage of decomposition.

Professor J. W. CAHN (Massachusetts Institute of Technology, Cambridge, U.S.A.): The invariant is shown in Fig. 4 of the paper by Tomozawa *et al.* This invariant measures the extent of decomposition, and it is still increasing with time. To be sure there is, as Professor Gerold points out, a large amount of decomposition initially. I think that this amount of decomposition is essential if you want to measure a decrease in amplitude, i.e., if you want to measure a reversion of the short-wavelength components. The scattered intensity is proportional to the square of the deviation from the mean composition and further precipitation is going on during the course of these experiments. Remember that we are testing here a diffusion equation which we use for spinodal decomposition, not the theory of spinodal decomposition itself. If we measure the two diffusion coefficients (equation (3) of my paper) in this way, then I believe we can be sure that we understand spinodal decomposition. I think Hilliard gave a very adequate reply to Professor Gerold's question in *Scripta Metallurgica.*‡

Professor C. S. BARRETT (University of Chicago, U.S.A.): Fig. 2 of the paper by Tomozawa *et al.* shows decreasing β at the cross-over point with increasing ageing time, but Cahn's theory predicts that this point should remain constant.

Professor CAHN: I do not understand this change in cross-over at all. Furthermore, if you look at Fig. 6 in the paper by Tomozawa *et al.* the straight lines have about the same gradient instead of the slope going through a maximum and then decreasing as β is increased. I am just as puzzled as you are.

Dr. M. TOMOZAWA, Professor H. HERMAN, and Dr. R. K. MACCRONE (University of Pennsylvania, U.S.A.) (*written reply*): We are in agreement with Professor Cahn's answer to Professor Gerold. This experiment was designed to test a diffusion equation and, though some decomposition has certainly taken place, a redistribution of wavelengths is occurring at the ageing temperature (or at the heat-treatment temperature, as it is referred to in glass science).

Regarding Professor Barrett's comment, we have indicated in the text of the paper that decomposition has apparently evolved to such a degree that one can no longer speak in terms of a linear theory. Rather, the establishment of significant composition gradients requires us to look at the contribution of higher-order terms in the equations. This has been considered by de Fontaine§ and recently by Tomozawa.‖ They conclude that the cross-over point should in fact shift to lower values of β, although a non-shifting cross-over point can still be observed if the scattering curves are taken at sufficiently small decomposition times.

If we are dealing with ideal conditions, i.e., very early in the process, it might be possible to observe a cross-over point that is invariant. However, there is at present no way of predicting for how long the cross-over point should remain at a constant angular position. In fact, the shift may begin after only a few per cent. of decomposition.

The important question of the influence of the higher-order terms will be considered in a later publication.

Miss J. M. SILCOCK (Central Electricity Research Laboratories, Leatherhead): Referring to Fig. 2 in the paper by Phillips, do the sidebands always show a greater intensity on the low-angle side?

Dr. V. A. PHILLIPS (General Electric Research Laboratories, Schenectady, U.S.A.): No, there is no consistent pattern of this kind. If you look at one of the sidebands you will notice that it is spotty. This is because the sample is relatively coarse-grained, which is one of the difficulties of using high-purity thin foils for X-ray work. The intensity of a sideband varies from place to place along the arc and I think this is due to an orientation effect, i.e., one grain is not giving the same intensity as another because of slight deviations from the Bragg angle. This means that one has either to use a powder sample as has been done previously or to use single crystals for more discriminating X-ray work.

Professor H. KIMURA (Tohoku University, Japan): Did Professor Gerold calculate the number of jumps made by the quenched-in vacancies before annihilation?

Professor GEROLD: No, we did not, but we should do so. (*Written reply*): With a Debye frequency of $10^{13}\,\mathrm{sec}^{-1}$ and neglecting an entropy term, the number of jumps amounts to 3×10^{7}–10^{8}, which is reasonable.

Mr. M. H. JACOBS (Tube Investments Research Laboratories, Cambridge): I should like to ask Dr. Wilson whether there is any difference in the kinetics of formation of G.P. zones and γ' in his steel.

* K. B. Rundman and J. E. Hilliard, *Acta Met.*, 1967, **15**, 1025.
† V. Gerold and W. Merz, *Scripta Met.*, 1967, **1**, 33.
‡ J. E. Hilliard and K. B. Rundman, *ibid.*, 1967, **1**, 37.

§ D. de Fontaine, Ph.D. Thesis, Northwestern University, **1967.**
‖ M. Tomozawa, Ph.D. Thesis, Univ. Pennsylvania, **1968.**

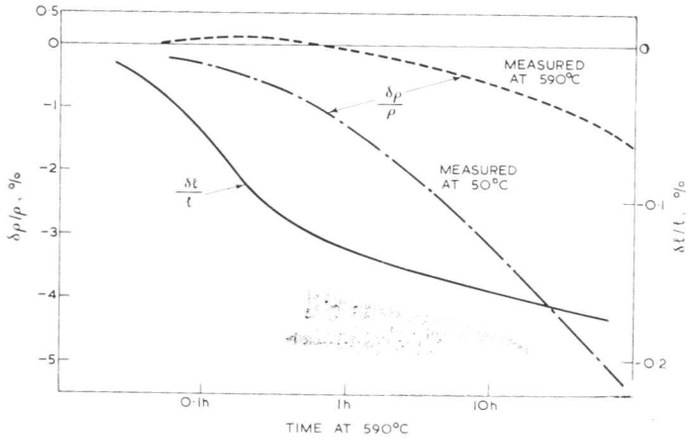

Fig. D.I.1 Electrical resistance (ρ) and length (l) changes in Fe–13% Cr–34% Ni–2·8% Al on ageing at 590° C. (Silcock.)

Dr. F. G. Wilson (British Steel Corporation, Rotherham): At 860° C, for example, there is an incubation period before the γ' phase (i.e., f.c.c. Ni_3Ti) is detected, whereas at lower temperatures, 700° C for instance, there is a spontaneous decomposition. We cannot determine the structure immediately, as we are unable to get superlattice spots from these clusters or zones until after 10 min ageing. Although the G.P. zones and γ' are structurally alike, I have made this, perhaps artificial, differentiation because there is a clear kinetic change. One is a nucleation and growth process and the other is spinodal decomposition.

Miss Silcock: Incubation periods are not obtained at low ageing temperatures on dilatometric examination of austenitic steels containing Al and Ti. The contraction commences immediately the material reaches the ageing temperature. High-temperature resistivity measurements tend to isolate the anomalous rise part of the resistivity change, since at high temperatures the variation of resistance with solute content is smaller than at low temperatures in these steels. Measurements at low temperatures show a decrease in resistance due to the decrease in solute content of the matrix, but owing to the superimposition of the anomalous rise the resistance changes are retarded as compared with length changes. With higher Al contents the resistivity change with solute content is greater, so that with a steel containing no Ti and 2·8 wt.-% Al only a small increase, followed by a more pronounced decrease, in resistance occurs even in measurements made at the ageing temperature (Fig. D.I.1). The anomalous rise appears to be associated with a critical size of γ' and so is dependent on the growth rate and not simply on the volume fraction of γ' formed, as is the length change. The " time for start of zone formation " on Fig. 7 is surely the " time for some γ' to reach the critical size ", but it appears that a wide range of sizes can give a resistivity increase. At 700° C γ' is easily observed by electron microscopy but at 500° C it is not. The matrix lattice parameter decreases even though the γ' particles are too small to be seen, and decreases in specimen length and in matrix lattice parameter occur before the increase in resistance.

Dr. Wilson: Is the resistivity measured at the ageing temperature, or at room temperature?

Miss Silcock: It is measured at the ageing temperature.

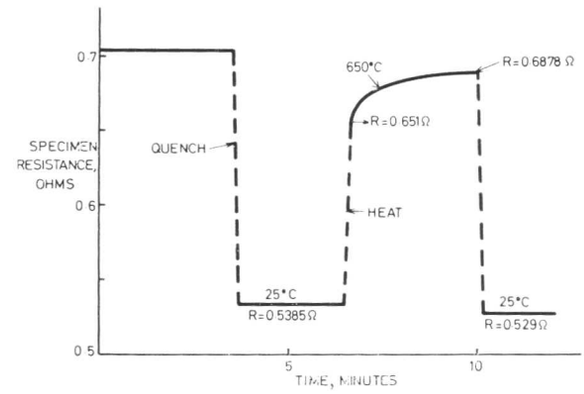

Fig. D.I.2 Resistance changes during ageing when measured at 25 and 650° C. (Wilson.)

Dr. Wilson: I cannot comment on the dilatometer results because I have recorded none myself but I should like to comment on the effects of measuring temperature on the resistivity. If we have some means of measuring resistance at the ageing temperature and also at room temperature, then this throws some light on previous measurements that have been made in age-hardening alloys. Most workers measure the resistance at room or sub-zero temperature, age at the high temperature, and then quench back down to room temperature to measure the resistance change.

I will not go into my experimental technique, but Fig. D.I.2 shows a typical result. The first point on the curve gives the resistance at the solution-treatment temperature, which is ~ 0·7 Ω. On quenching to 25° C the resistance is 0·5385 Ω. On heating rapidly to the ageing temperature and then ageing continuously, the resistance increases quite markedly by ~ 5%. But if we then quench the specimen to room temperature we find that there is a decrease in the resistance from the original value of the solution-treated specimen.

What this indicates is that the temperature coefficients of resistance of the aged and solution-treated alloys are different. It is absolutely vital that measurements should be made at the ageing temperature. If you measure at room temperature you are going to be led astray.

Professor R. B. Nicholson (University of Manchester): This point in Wilson's paper where the maximum rate of zone formation is identified as the spinodal temperature seems to me to be not strictly valid. Just below the spinodal, the only stable wavelengths are very long ones, and there is an apparent incubation period because the atoms have to diffuse over such long distances. If you are measuring a particular difference in composition with your experimental technique it will take longer just below the spinodal than it will well below the spinodal, because of these long wavelengths. I wonder in this instance whether it is really justifiable to say that the maximum rate of decomposition occurs at the spinodal temperature.

Dr. Wilson: Certainly, at the lower temperatures I do not think there is any doubt that the limiting factor is the diffusion of solute. This is why there is such a long incubation period. I do not know whether the term " incubation period " should be used here. This was associated with nucleation and growth.

Professor Cahn asked earlier for a system limited by slow spinodal decomposition. Maybe this is it. If you quench

to a low enough temperature, of the order of 400 or 500° C, the result is that there is a slow zone formation. If you look at corresponding thin foils, you cannot see any precipitation or any zone formation. For instance, at 500° C after ~ 1000 min, which corresponds to the maximum resistivity, there is no indication of the presence of zones. This point is not really made clear by Miss Silcock's interpretation of the resistivity results.

Professor CAHN: Hilliard, Huston, and I wrote a paper* on spinodal decomposition during continuous cooling and part of this paper was the calculation of a C curve for the spinodal. There is a simple formula:†

$$\frac{\Delta T}{T_s} = \frac{2RT}{Q}$$

where ΔT is the undercooling below the spinodal at the nose of the C curve, T_s is the spinodal temperature, and Q is the activation energy for diffusion. If you apply that formula to Fig. 7 of Wilson's paper you come up with a figure for Q of ~ 70 000 calories. This is quite a reasonable value for diffusion.

Dr. P. WILKES (University of Manchester): I should like to ask Professor Cahn if it is possible to regard spinodal decomposition and G.P. zone formation as limiting cases of nucleation and growth? G.P. zone formation would then be when the nuclei are very small, and spinodal decomposition would arise when the nuclei do not have a definite boundary but a diffuse interface. Is it possible to look at it meaningfully in this way?

Professor CAHN: No, I do not think so. But I do think G.P. zones are quite possibly spinodal decomposition way off on one side of the phase diagram. It *is* spinodal decomposition, but with a very small volume fraction. In that region the diffusion coefficient is changing very rapidly because, after all, it changes sign at the spinodal and you cannot use the simple linear solution for very long. De Fontaine‡ has done a diffusion calculation for spinodal decomposition in the immediate vicinity of the spinodal when it is well to one side of the phase diagram. The solution decomposes asymmetrically and he gets computer results which are very much like G.P. zones.

There is quite a distinction between nucleation and growth compared with spinodal decomposition. This goes back all the way to Gibbs; he in fact looked at spinodal decomposition first. He simply considered the possibility of what is necessary for a phase to be metastable. He found that outside the spinodal the phase could be metastable; a second phase could form eventually but there was some barrier to its formation. Inside the spinodal, however, there was no such barrier; the decomposition was quite simple. I think it is much simpler than nucleation and growth. The instant you get outside the spinodal you have to look for a barrier, diffusion is normal (i.e., it is positive), and so the situations are quite distinct. I do not think there is any similarity.

Mr. R. D. GARWOOD (University of Cardiff): I wonder if Professor Nicholson is quite certain that continuous recrystallization and/or grain growth of the quenched Zn–Al eutectoid alloy does not occur at room temperature. I think that the structure shown in Fig. 6 of the paper by Ardell *et al.* may be the result of a secondary process taking place after the alloy has transformed by a discontinuous or cellular reaction.

Professor NICHOLSON: No, if one is very successful with the quench and the spinodal process has not gone very far by the time the specimen is put in the microscope, it does decompose in a lamellar way starting at the surface of the specimen and one gets a very fine lamellar decomposition product. This is quite stable as lamellae, so I do not think that the structure in Fig. 6 is produced by spheroidization.

Professor CAHN: Is it possible that for the non-eutectoid alloys, one is crossing the spinodal at almost the same time as the coherent phase boundary?

Professor NICHOLSON: Yes, I think it is perfectly possible. The two curves could be within ~ 5 or 10 degC of each other. I agree that this could well be an explanation of the modulated structures of the non-eutectoid alloys. This close proximity of the two curves is well illustrated by Professor Gerold's paper. We could only say from our experiments that we had crossed the coherent phase boundary but we may well have crossed the spinodal at the same time.

---

* E. L. Huston, J. W. Cahn, and J. E. Hilliard, *Acta Met.*, 1966, **14**, 1053.
† J. W. Cahn, *Trans. Met. Soc. A.I.M.E.*, 1968, **242**, 166.
‡ D. de Fontaine, *loc. cit.*

Nucleation in Solids: (A) Brief Survey; (B) Cellular Precipitation*

K. N. Tu and D. Turnbull

The simple theory for nucleation in solid–solid transformations is briefly surveyed, with special emphasis on the key role of crystallographic misfit. Observations on the development of the lamellar morphology of tin precipitated from lead–tin solid solutions are reviewed and interpreted.

Brief Survey

Christian[1] has reviewed this subject comprehensively and critically. The present authors survey here some features of special interest.

In a first-order solid-state phase change, $\alpha \rightarrow \beta$, the mode of transformation and the departure from equilibrium required for a measurable rate of initial formation of β within perfectly crystalline α are expected to depend critically upon the crystallographic misfit between the two phases. More specifically, in those precipitation processes in which there is a continuity of states between α and β, the range of conditions where the spinodal mode is possible should be greater the smaller is the misfit. In nucleation and growth processes the departure from equilibrium required for measurable homogeneous nucleation of β should, on the basis of nucleation theory, rise sharply with misfit. These effects reflect the expected marked dependence on misfit of coherency strain energy and of the interfacial tension, $\sigma_{\alpha\beta}$, between unstrained α and β.

The variation of $\sigma_{\alpha\beta}$ with misfit has been deduced from dislocation models for interphase boundaries.[2,3] Where the misfit is very large or the dislocation model is inapplicable, it has been inferred intuitively that the magnitude of $\sigma_{\alpha\beta}$ will approximate that of the tension of high-angle grain boundaries in the α or β phase. If the compositions of α and β are different, there may be a chemical, $\sigma^c{}_{\alpha\beta}$, as well as a misfit contribution, $\sigma^s{}_{\alpha\beta}$, to the interfacial tension. For small misfits we expect that[4]

$$\sigma_{\alpha\beta} \simeq \sigma^s{}_{\alpha\beta} + \sigma^c{}_{\alpha\beta}$$

According to simple nucleation theory the frequency of homogeneous nucleation of unstrained β should be related to $\sigma_{\alpha\beta}$ by the equation

$$I \simeq n_v x^2 k_1 \exp\left[-b\,(\sigma_{\alpha\beta})^3/(\Delta G_v)^2 kT\right] \text{ volume}^{-1} \text{ time}^{-1} \quad \ldots (1)$$

where n_v is the number of atoms per unit volume in the α phase, x is the mole fraction of β composition in α, k_1 is the jump frequency across the α/β interface, ΔG_v is the change in Gibbs free energy in the transformation per unit volume, b is a constant depending on the shape of the nucleus, and it is supposed that $\sigma_{\alpha\beta}$ is constant over the surface of the nucleus. Thus, the nucleation frequency falls as the exponential of the cube of $\sigma_{\alpha\beta}$.

The predictions of this simple theory for the effect of misfit on the nucleation frequency have been described elsewhere.[1,4,5] The general conclusion is that for all but the smallest misfits (e.g. < 2–3% differences in atomic spacings) quite large departures from equilibrium should be required for measurable homogeneous nucleation of *unstrained* β in α. When the misfit is very large, homogeneous nucleation should sometimes not be measurable under any conditions owing to negligibly small values of k_1 at the departures from equilibrium required for appreciable values of the exponential term in $\sigma_{\alpha\beta}$.

The structural contribution to the interfacial tension can be greatly reduced or eliminated entirely when the β and its surrounding matrix are suitably strained. This effect is probably the most common motivation for the development of transformation strains. At small values of the equilibrium misfit δ, the β nucleus is likely to form coherently since the strain energy required to eliminate the structural part of $\sigma_{\alpha\beta}$, which rises rapidly with δ at low δ, is relatively small.

When β forms incoherently the magnitude of the transformation strains that develop will depend on the rates of interface or diffusion processes relative to the rates of strain relief by processes such as dislocation generation and movement and vacancy diffusion. For example, in precipitation processes one of the principal methods for relieving strain is by diffusion of vacancies to the interface. If precipitation is limited by diffusion via a vacancy mechanism, appreciable transformation strains are not likely to arise during nucleation since the time constant for relieving them will be of the same order as that for precipitation. However, if the precipitation were effected by rapid interstitial diffusion from a dilute solution, large transformation strains could develop in the nucleation and early growth stage.

Cahn and Hilliard[6] showed that the chemical part of the interfacial tension should vanish within the composition range delineated by the spinodal curves. Thus, within this range there should be no thermodynamic barrier to the initiation of precipitation on a relatively fine scale. The departures from

Manuscript received 1 April 1968. K. N. Tu, Ph.D., and Professor D. Turnbull, Ph.D., are in the Division of Engineering and Applied Physics, Harvard University, Cambridge, Mass., U.S.A.

*This section of the paper was presented and discussed in Session VI.

equilibrium required to reach the spinodal range increase rapidly at all compositions with increasing misfit. Cahn[7] has developed the theory for this effect.

In summary, simple nucleation theory seems to rule out measurable homogeneous nucleation in first-order solid-state phase changes at small departures from equilibrium and even at extremely large departures from equilibrium for the nucleation of phases that are partly or wholly incoherent. We suppose that the nucleation which, in fact, usually occurs quite close to equilibrium in these cases is heterogeneous in nature. The common heterogeneous nucleation sites in solid-state transformations are free surfaces, grain and interphase boundaries, grain edges and corners, and dislocations. Heterogeneous nucleation is recognized by its localization at these sites and sometimes by its scale, since the spacing of heterogeneities in well-annealed crystals is not likely to be $< 10\,\mu m$.

Experience on the effect of misfit on the kinetics of solid-state transformations appears to be in qualitative agreement with the predictions of simple nucleation theory. However, the interpretation of results is sometimes complicated by difficulty in distinguishing between resistance to the formation or to the motion of the interface in transformations.[8] For example, the f.c.c. $\rightarrow$ h.c.p. transformation in cobalt does not occur at a measurable rate in small single crystals even though the misfit across the close-packed planes is very slight. It appears that the high resistance to transformation in this case results from the unavailability of dislocations which are required for motion of the interface at appreciable rates. This may also be the explanation for the high resistance of small single crystals of f.c.c. iron alloys to the interior nucleation of the b.c.c. phase at low temperatures, though here the relatively large misfit should also make homogeneous nucleation difficult.

A more definitive assessment of the role of misfit in nucleation can be made from experience on phase changes at temperatures high enough for substitutional diffusive mechanisms of interface motion and strain relief to occur at appreciable rates. Most experience of this sort is from studies of the precipitation of substitutional solutes from solid solution and it is in qualitative agreement with the prediction that the resistance to both homogeneous nucleation and spinodal decomposition should increase sharply with increasing misfit. For example, the spinodal mechanism occurs readily in systems such as Al–Zn[9,10] and Au–Pt,[9] in which the misfit is relatively small. However, the Au–Ni system,[9] in which the misfit is large, exhibits a very high resistance to the homogeneous initiation of precipitation.

Studies[11] of the kinetics of precipitation of cobalt from dilute solutions of cobalt in copper indicate that the nucleation frequency is negligible at small deviations from equilibrium, but it rises sharply to large values when the supersaturation ratio rises to values above 1·5–2·0. Cobalt particle densities of 10^{12}–$10^{17}/cm^3$ are reached. This large particle density and its mode of development are characteristic of a copious homogeneous process, which is expected for this system in view of the small misfit of $< 2\%$.

On the other hand, it appears that the nucleation of phases that fit poorly with their parent solutions is infrequent and generally heterogeneous in nature even at large departures from equilibrium. For example,[12] the nucleation of the diamond cubic phase of silicon from dilute solutions of silicon in aluminium apparently occurs only heterogeneously, at least at all supersaturation ratios $<$ 10–20. Another example is nucleation of the tetragonal phase of tin from f.c.c. solutions of tin in lead, which is localized principally at interfaces within the solution under most conditions.

After this brief survey of the general subject of nucleation in solids, we now turn to a more specific topic: the nucleation and growth at grain boundaries of precipitate lamellae which give rise to cellular precipitation.

Cellular Precipitation

In cellular precipitation a semi-coherent precipitate generally of the equilibrium phase, forms at a solid-solution (α) grain boundary which is carried along by the growing precipitate.[13] The precipitate usually takes the form of separated parallel lamellae, grouped into colonies or cells. Precipitate growth can be and often is effected almost wholly by the diffusion of solute along the moving cell boundary which is at the same time an α–α grain boundary. The boundary may also play a key role in facilitating the nucleation of the precipitate.

Two of the principal questions about the process are: how is it initiated at the grain boundary, and what is the mechanism whereby the multiplication of lamellae occurs to form a given colony?

The investigations made of the crystallographic orientation relations in the process indicate that a given set of parallel lamellae within a colony exhibit a single and well-defined crystallographic orientation and habit with respect to the solid-solution grain in which they are embedded. For example, Speich[14] reported that Ni_3Ti lamellae precipitate from an austenitic Fe–Ni–Ti alloy with the habit $(111)_\gamma$ and the orientation relation $(001)_{Ni_3Ti} \parallel (111)_\gamma$ and $[010]_{Ni_3Ti} \parallel [\bar{1}10]_\gamma$. We have found[15,16(a)] that the habit plane of tin lamellae precipitated from f.c.c. lead-rich solutions is one of the {111} planes of the lead and the orientation relation is $[001]_{Sn} \parallel \langle 110 \rangle_{Pb}$ and $\{310\}_{Sn} \parallel \{111\}_{Pb}$. This relation was manifested by a sharp single-crystal Laue pattern, which also indicates that only one of the four sets of $\{111\}_{Pb}$ planes and one of the three $\langle 110 \rangle_{Pb}$ directions are selected by a particular family of parallel lamellae. Often, however, two or more families of lamellae, with mutually perpendicular habits, are observed on $(100)_{Pb}$ within a single cell.

The lamellae in a single family may have formed either from a single initial lamella by a branching mechanism or by the nucleation in the special orientation of each individual lamella in the family. It appears, for example, that a branching mechanism is principally responsible for the lamellation within a pearlite colony.[17] However, our microscopic observations[15,16(b)] on the formation of tin cells from lead–tin solutions strongly support the conclusion that in this case each member of a family of lamellae nucleates individually at the boundary. The evidence is as follows: (1) In the early stages of precipitation many lamellae in the special orientation appear, rather widely separated and with no apparent interconnection, along the grain boundary. (2) Several of the earliest members of a family of lamellae extend all the way back from the cell boundary to its starting position. (3) No interconnections between lamellae were observed in the successive surfaces exposed as a cell was sectioned.

A family of tin lamellae appears to develop by the following sequence.[16(b)] (1) A tin particle nucleates along the boundary in the special orientation relation with *one* (say α_1) of the solid-solution grains forming the boundary. This means that the boundary (it was a symmetrical tilt-type boundary separating grains misoriented by rotation through an angle θ around a [100] axis) must have been deformed locally to a position parallel with the habit plane of α_1 since it will not, on the average, lie in the special position. This deformation may

be in the boundary initially as a result of a local pinning or it may occur during the nucleation. (2) The particle grows along the boundary, which deforms concurrently, to a macroscopic size. (3) The tin plate is then embedded entirely in α_1 by a " replacive " motion of the grain boundary. This leaves the newly formed section of the boundary roughly parallel with the habit plane of the tin plate and thus in the position most favourable for the nucleation of the second lamella in the special orientation relation with α_1. (4) A second plate nucleates along this new section of the boundary and grows parallel with the first. This sideways addition of plates is repeated to form a family of lamellae. During cell growth new lamellae sometimes appear between those already formed, as well as at the cell edge. We have suggested that this might occur when the moving boundary passes over an obstacle that would temporarily deform it into an orientation favourable for nucleation of the special orientation.

We have also noted that tin particles which are not in the special orientation appear along the grain boundary, frequently when the boundary is stationary and rather infrequently when it is moving. These non-special particles are always left behind by the moving boundary to constitute a " debris " between the lamellae. However, these results show that we must consider the possibility of growth as well as nucleation selectivity to account for the special orientation of the lamellae.

The special orientation is one that can result in a semi-coherent interface, with a relatively small misfit, between the tin and α_1. Thus, the corresponding interfacial tension, σ_1, is expected to be relatively small and possibly a cusped minimum. Aaronson and Liu[18] have estimated from correlations that $\sigma_1 \simeq 125$ ergs/cm^2 for the lead–tin system. We have formulated the free energy of formation of a disc in the special orientation lying along a boundary, which has been deformed locally through an angle φ to be parallel with the habit plane of α_1, as follows:[15,16(b)]

$$\Delta G = \pi r^2 t \Delta G_v + \pi r^2 f(\varphi) + 2\pi r t \sigma_3 \qquad \ldots (2)$$

where

$$f(\varphi) = \sigma_1 + \sigma_2 - \frac{1 - \sin\varphi}{\cos\varphi}\sigma_{\alpha\alpha} \qquad \ldots (2a)$$

and r is the radius of disc, t is the thickness of disc, σ_2 is the interfacial tension between the disc and the grain α_2, $\sigma_{\alpha\alpha}$ is the interfacial tension between the solid-solution grains α_1 and α_2, σ_3 is the interfacial tension at disc edges. See Ref. 16(*b*), Fig. 6, for definition of φ. According to simple nucleation theory the critical free energy for forming a special nucleus is then

$$\Delta G^* = \frac{4\pi\sigma_3^2 f(\varphi)}{\Delta G_v^2} \qquad \ldots (2b)$$

$f(\varphi)$ may take on values ranging between $\sigma_1 + \sigma_2$ (for $\varphi = 90°$) and $\sigma_1 + \sigma_2 - \sigma_{\alpha\alpha}$ (for $\varphi = 0$).

If, indeed, the special orientation is at an energy cusp then $\sigma_2 > \sigma_1$ and the difference in tension $\sigma_2 - \sigma_1$ would supply some of the motivation that embeds the tin lamellae in α_1.

It is likely that the energy of the $\alpha_1\alpha_2$ grain boundary depends significantly on the concentration of tin in the boundary region. Thus, this energy may be varying considerably in the dynamic situations in which the boundary is moving, as during deformation, replacive motion, or cell growth.

The relatively small proportion of tin particles in the special orientation along the initially stationary boundary probably reflects the difficulty of deforming the boundary through the angle φ. Indeed, the specially oriented particles may have nucleated only on parts of the boundary that had been deformed locally through obstacle pinning to positions nearly parallel with the special habit plane.

We have noted, however, that after the replacive motion is completed the deformation angle, φ, for nucleation on the newly formed section of the $\alpha_1\alpha_2$ grain boundary is practically zero. Thus $f(\varphi)$ for this boundary is reduced almost to $\sigma_1 + \sigma_2 - \sigma_{\alpha\alpha}$ and nucleation on it of a specially oriented plate is especially facilitated. Consequently, the appearance of one such lamella is likely to be followed by the formation of an entire family of lamellae by sideways addition. Since the boundary is, after each replacive motion, parallel with the habit plane of the initial lamella, all lamellae within a family should exhibit just one of the four sets of habit planes, as is observed. The tension, σ_2, between the tin lamella and the α_2 grain should also be somewhat dependent upon the α_2–tin orientation relation. Dr. G. H. Bishop has suggested to us that the particular direction from the set of the 3 $\langle 110 \rangle_{Pb}$ selected by a family of lamellae may be that for which σ_2 is a minimum.

Plates in the special orientation are sometimes observed[15,16(b)] along low-angle grain boundaries which appear to have grown from the boundary with both plates embedded in a grain. Aaronson and Liu[19] have taken this result to indicate that special particles would have nucleated homogeneously at an appreciable rate except for the sluggishness of the tin diffusion in the lattice. The growth of the plates from the boundary was probably effected principally by diffusion of tin along the grain boundary and along the tin/lead interfaces. For the nucleation, however, there is the alternative possibility that it was facilitated by inclusions lying along the boundary.

As we have noted, many particles not in the special orientation are nucleated along the boundary and almost always left behind by the moving cell boundary. The slow growth rate of the non-special particles may be due in part to the relatively higher tension of their interfaces with lead, compared with σ_1 for the special habit plane, which would necessitate a larger proportion of the motivating free energy for precipitation for the formation of interfaces. Also the special orientation might be especially favoured for growth since its growth direction, $[001]_{Sn}$, is parallel with a screw axis. This should assure that a high proportion of the atom sites on the lamellae edges should be favourable for the reception of tin atoms.

Thus, the orientation is specially favourable for the replacive motion that embeds the lamellae within a grain and for the continued growth of the cell. Its growth also imposes a boundary deformation that favours nucleation of special lamellae and thus the development by individual nucleation of a family of lamellae.

Only a part, Q, of the supersaturation of the solution is relieved by the isothermal passage of the cell boundary. Q is defined by

$$Q = \frac{c_0 - c'}{c_0 - c_e}$$

where c_0 is the initial concentration of solute, c' is the average concentration of solute after the forward passage of a cell boundary at temperature T, and c_e is the equilibrium concentration of solute at temperature, T. In the cellular precipitation of tin from lead, values of Q ranging from 0·4 to 0·6, depending on temperature, have been reported.

A solution with a uniform concentration c', as defined above, would be in equilibrium with tin at temperature T'. One of the authors[15] has observed that when the system is heated to above T' the cell boundaries recede, with complete dissolution of the tin in the volume through which they move, while the lamellae on the opposite sides of the boundaries remain unchanged in appearance.

The interlamellar spacing, S, will be limited by the frequency of nucleation of lamellae on the cell boundaries and ultimately by the free energy, ΔG, released in the precipitation. Zener[20] and Cahn[21] developed the theory for the case in which the latter condition is limiting. They obtained

$$R\,\Delta G = \frac{2\sigma_1 \bar{V}}{S} \qquad \ldots (3)$$

where $\bar{V}$ is the molar volume, which is assumed to be the same for the solution and the precipitate, and R is the fraction of ΔG that goes into the interfacial tensions. Cahn[21] showed that R should be 2/3 for boundary-diffusion-limited growth.

Usually the observed interlamellar spacing (e.g. Aaronson and Liu[19]) is substantially larger than the Zener limiting value. Also rather large variations in spacing within a cell, depending on the angle between the habit plane and the cell boundary, are sometimes observed.[15] A striking example of such a variation is shown in Fig. 1. This shows a cell growing at room temperature which had originated at a 37° tilt boundary (around a [100] axis) between two bicrystals. The spacing between lamellae with (100) traces perpendicular to the boundary is ~ 3 times that of the lamellae with (100) traces which are more nearly parallel with the boundary. Note that many more of the lamellae in the second set than in the first set have apparently broken off from the moving boundary. The much larger spacing in the set with nearly perpendicular traces would seem to reflect the larger deformation angle, φ, required for the nucleation of the lamellae in the set.

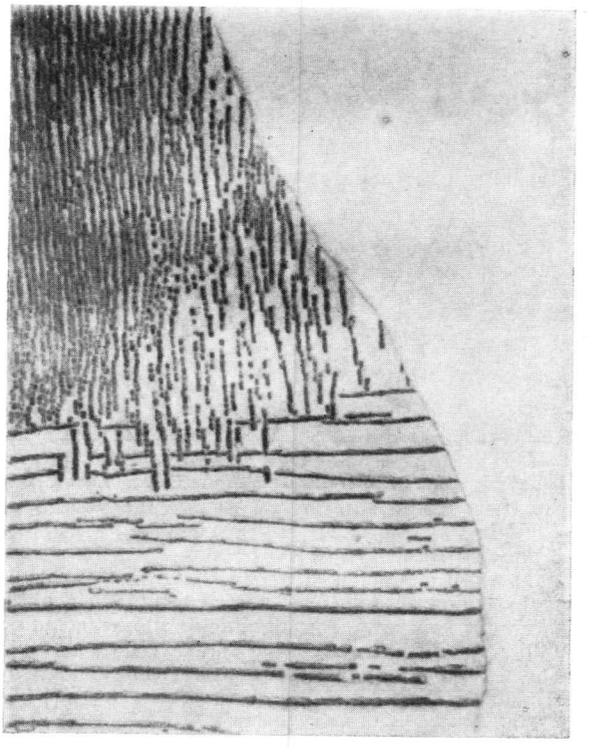

Fig. 1 Photomicrograph of a cell showing the different spacings exhibited by two families of lamellae. The surface is parallel to the $(001)_{Pb}$ *plane of a bicrystal (initially 94·5% Pb, 5·5% Sn) misoriented by a rotation of* 37° *around a* $(100)_{Pb}$ *axis.* × 400.

Acknowledgement

The research at Harvard University discussed in this paper was supported in part by the Advanced Research Projects Agency under Contract ARPA–SD–88.

References

1. J. W. Christian, "The Theory of Transformations in Metals and Alloys". **1965:** Oxford, &c. (Pergamon Press).
2. J. H. van der Merwe, *Proc. Phys. Soc.*, 1950, [A], **63,** 613.
3. H. Brooks, "Metal Interfaces", pp. 20–65. **1952:** Cleveland, Ohio (Amer. Soc. Metals).
4. D. Turnbull, "Impurities and Imperfections", pp. 121–145. **1955:** Cleveland, Ohio (Amer. Soc. Metals).
5. D. Turnbull, "Solid State Physics", Vol. 3, pp. 226–310. **1956:** New York and London (Academic Press).
6. J. W. Cahn and J. E. Hilliard, *J. Chem. Physics*, 1958, **28,** 258.
7. J. W. Cahn, *Acta Met.*, 1961, **9,** 795.
8. Ref. 4, p. 132; Ref. 5, pp. 294–298.
9. For summary, see Ref. 1, pp. 614 *et seq.*
10. K. B. Rundman and J. E. Hilliard, *Acta Met.*, 1967, **15,** 1025.
11. I. S. Servi and D. Turnbull, *ibid.*, 1966, **14,** 161.
12. H. S. Rosenbaum and D. Turnbull, *ibid.*, 1958, **6,** 653; 1959, **7,** 664.
13. For a general review, see Ref. 1, pp. 454–470, 643–649.
14. G. R. Speich, *Trans. Met. Soc. A.I.M.E.*, 1963, **227,** 754.
15. K. N. Tu, Ph.D. Thesis, Harvard Univ., **1968.**
16. (*a*). K. N. Tu and D. Turnbull, *Acta Met.*, 1967, **15,** 369; (*b*). *ibid.*, 1967, **15,** 1317.
17. M. Hillert, "Decomposition of Austenite by Diffusional Processes", p. 197. **1962:** New York and London (Interscience Publishers).
18. H. I. Aaronson and Y. C. Liu, *Ford Motor Co. Scientific Lab. Rep.* (**SL67-34**), 1967.
19. H. I. Aaronson and Y. C. Liu, *Acta Met.*, in the press.
20. C. Zener, *Trans. Amer. Inst. Min. Met. Eng.*, 1946, **167,** 550.
21. J. W. Cahn, *Acta Met.*, 1959, **7,** 8.

The Nucleation of Precipitates in Aluminium Alloys

G. W. Lorimer and R. B. Nicholson

A new theory of precipitate nucleation is developed. The basic features of the theory are the growth of G.P. zones at low ageing temperatures and the ability of these to transform to precipitates when the ageing temperature is suddenly raised. The theory explains all the major phenomena observed in homogeneously distributed precipitates in aluminium alloys, including grain-boundary structures and the effects of multiple heat-treatments. Examples are given from the systems Al–Cu and Al–Ge.

The classical theory of nucleation of a phase transformation was developed for a vapour → fluid change but has been presented in modified form for a solid → solid change.[1] While the theory is successful in making quantitative predictions about the nucleation rate in some simple systems, e.g. Cu–Co,[2] it is able to deal only qualitatively with the effects of lattice defects and it has also failed to predict the complexities observed in the formation of the so-called "homogeneous" precipitates in age-hardening alloys. The latter failure has been particularly noticeable in the last few years as a result of work on precipitate structures near grain boundaries and the investigation of multi-stage heat-treatments.[3–9] It has become apparent that the normal "homogeneous" precipitation, and hence the normal properties of an alloy, can be varied over a very wide range by seemingly insignificant changes in heat-treatment procedure in a way that would not be expected from the application of classical nucleation theory to the problem.

In the present paper we outline the development of ideas expressed in earlier papers by Embury and Nicholson[3] and Lorimer and Nicholson[7] and apply them to a new study of precipitation in Al–Ge and the best-known of all age-hardening systems, Al–Cu.

Experimental

The work was carried out using Al–3·9 wt.-% Cu and Al–4·5 wt.-% Ge alloys prepared from superpurity-base aluminium.* The Al–Cu system precipitates the well-known G.P. zones, θ″ and θ′, as transition phases before the equilibrium θ ($CuAl_2$). In the Al–Ge system the diamond cubic Ge precipitate is preceded only by G.P. zones.[10]

* The authors are grateful to the British Aluminium Co. Research Laboratories for supplying these alloys.

Manuscript received 24 April 1968. Professor R. B. Nicholson, M.A., Ph.D., and G. W. Lorimer B.A.Sc., Ph.D., are in the Department of Metallurgy, Faculty of Science, University of Manchester.

A Nucleation Model

We consider a solid solution A–B in which the precipitation sequence is:

$$\alpha_{\text{supersat.}} \rightarrow \alpha'_{\text{sat.}} + \text{G.P. zones} \rightarrow \alpha_{\text{sat.}} + \beta$$

where α and β are the two terminal solid solutions and G.P. zones, defined as a stable coherent segregate of B atoms in the A matrix, are formed as a transition precipitate. Since G.P. zones are less stable than β, the concentrations of the two solid solutions in equilibrium with the two phases is such that $\alpha'_{\text{sat.}} > \alpha_{\text{sat.}}$

Neglecting G.P. zone formation and considering only the nucleation frequency of the β phase I_β, classical nucleation theory predicts that the I_β is given by

$$I_\beta = K_1 \exp\left(-\frac{\Delta G_c^\beta}{kT}\right) \exp\left(-\frac{Q_m}{kT}\right) \quad \ldots (1)$$

where K_1 is a factor that includes the vacancy concentration; ΔG_c^β is the activation energy required to form the critical-sized nucleus of diameter d_c; kT has its usual meaning; and Q_m, the activation energy for migration of solute atoms, is involved because the formation of β in an α matrix necessarily requires changes in composition. Equation (1) is obtained from a consideration of the free-energy changes involved in nucleating a β particle in an α matrix by the formation of transient B-rich segregates in the α matrix to build up a "quasi-steady-state" distribution of embryos. Because of the rapid reduction of the value of ΔG_c^β as the supersaturation i increases ($i = c/c_e^T$, where c is the solute content of the alloy and c_e^T is the equilibrium concentration at a temperature T), the nucleation rate is a very strong function of the supersaturation, as shown in Fig. 1. It is conventional to define a critical supersaturation i_c (or undercooling, ΔT_c, from the solvus temperature T_β) where the homogeneous nucleation rate becomes significant in the context of the experiment. In the present case homogeneous nucleation becomes important if it exceeds the rate of heterogeneous nucleation, particularly on dislocations. Typically, a quenched crystal contains 10^8–10^9 cm.cm^{-3} of dislocation lines. The nucleation density is of the order of 10^5–10^6 particles per cm of dislocation and nucleation is complete in $\sim 10^2$ sec. This gives a critical nucleation rate for homogeneous nucleation, $I_\beta^{\min}$, of $\sim 10^{12}$ particles cm^{-3} sec^{-1}. In systems where the precipitate has a similar crystal structure and lattice parameter to the matrix, the value of ΔG_c^β is small and sensible homogeneous nucleation rates can be obtained with undercoolings of the